












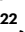


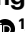
GWAS of multiple neuropathology endophenotypes identifies new risk loci and provides insights into the genetic risk of dementia

Received: 5 May 2023

Accepted: 30 August 2024

Published online: 8 October 2024

 Check for updates

Lincoln M. P. Shade¹, Yuriko Katsumata ^{1,2}, Erin L. Abner^{2,3}, Khine Zin Aung ^{1,2}, Steven A. Claas ¹, Qi Qiao^{1,2}, Bernardo Aguzzoli Heberle ^{2,4}, J. Anthony Brandon^{2,4}, Madeline L. Page ^{2,4}, Timothy J. Hohman ^{5,6}, Shubhabrata Mukherjee ⁷, Richard P. Mayeux ⁸, Lindsay A. Farrer ^{9,10,11,12,13}, Gerard D. Schellenberg^{14,15}, Jonathan L. Haines^{16,17}, Walter A. Kukull ¹⁸, Kwangsik Nho^{19,20,21}, Andrew J. Saykin ^{20,22}, David A. Bennett^{23,24}, Julie A. Schneider ^{23,24,25}, The National Alzheimer's Coordinating Center*, Mark T. W. Ebbert ^{2,4,26,28}, Peter T. Nelson^{2,27,28} & David W. Fardo ^{1,2,28} ✉

Genome-wide association studies (GWAS) have identified >80 Alzheimer's disease and related dementias (ADRD)-associated genetic loci. However, the clinical outcomes used in most previous studies belie the complex nature of underlying neuropathologies. Here we performed GWAS on 11 ADRD-related neuropathology endophenotypes with participants drawn from the following three sources: the National Alzheimer's Coordinating Center, the Religious Orders Study and Rush Memory and Aging Project, and the Adult Changes in Thought study ($n = 7,804$ total autopsied participants). We identified eight independent significantly associated loci, of which four were new (*COL4A1*, *PIK3R5*, *LZTS1* and *APOC2*). Separately testing known ADRD loci, 19 loci were significantly associated with at least one neuropathology after false-discovery rate adjustment. Genetic colocalization analyses identified pleiotropic effects and quantitative trait loci. Methylation in the cerebral cortex at two sites near *APOC2* was associated with cerebral amyloid angiopathy. Studies that include neuropathology endophenotypes are an important step in understanding the mechanisms underlying genetic ADRD risk.

Amnesic dementia, often diagnosed as late-onset Alzheimer's disease (LOAD), is increasingly recognized to be a heterogeneous clinical syndrome that may reflect multiple underlying heritable pathological processes^{1–3}. LOAD genome-wide association studies (GWAS) have primarily used clinical diagnosis or proxy phenotypes based on family history of dementia^{4–7}. While these GWAS have been immensely successful, identifying over 80 disease-associated genetic loci⁶, the use of clinical phenotypes complicates interpretation and partly obscures

the complex and common reality of mixed neuropathologies in aged individuals^{3,8}. To complement the successes from previous studies, GWAS using neuropathology endophenotypes (NPEs) is an essential next step to identify loci that drive specific Alzheimer's disease and related dementias (ADRD)-associated pathologic mechanisms⁹.

Amyloid plaques and neurofibrillary tangles (NFT), together known as Alzheimer's disease (AD) neuropathologic changes (ADNC), are present at autopsy in most brains from patients diagnosed

A full list of affiliations appears at the end of the paper. *A full list of authors can be found at the end of the article. ✉e-mail: david.fardo@uky.edu

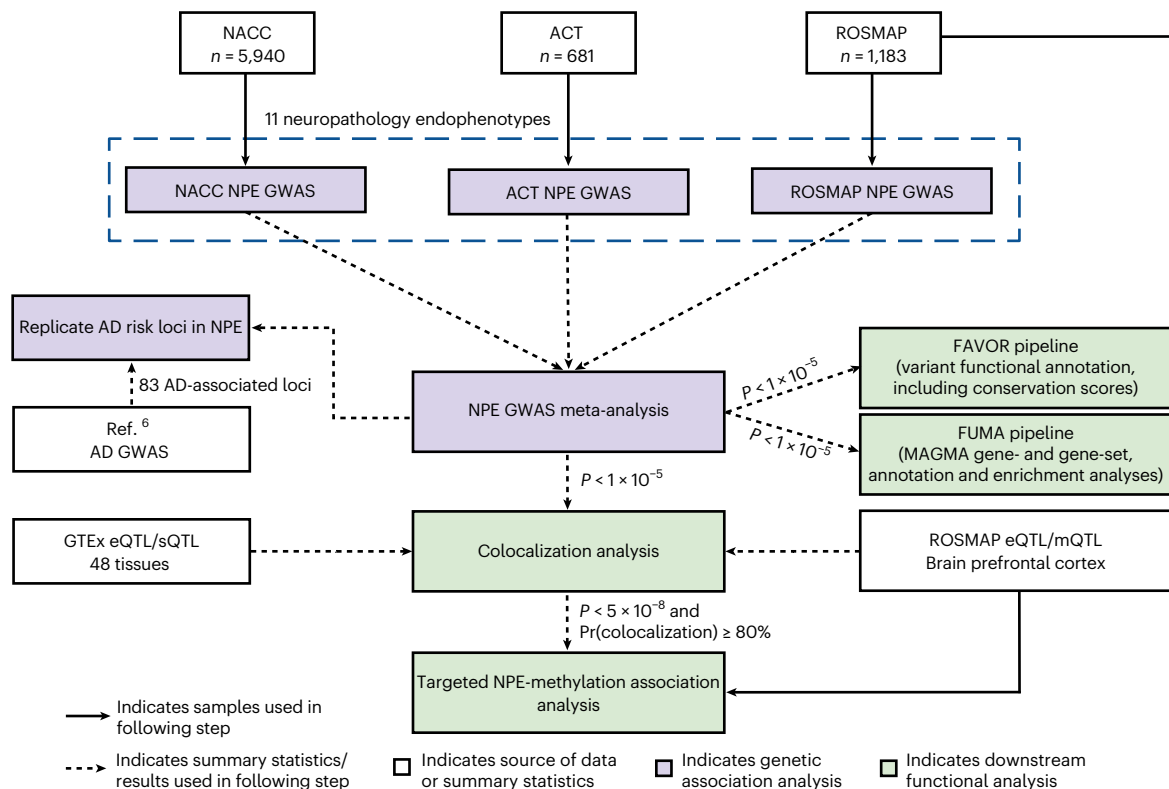


Fig. 1 Overview of GWAS meta-analysis study design. We performed GWAS meta-analyses of 11 NPEs across three data sources. White boxes represent data sources or summary statistics used in this study. Purple boxes represent individual steps throughout the genetic association analysis, and green boxes represent downstream functional analyses. The first stage of this analysis involved independent GWAS performed in parallel across the NACC neuropathology dataset, the ACT study and the combined ROSMAP. We then performed a meta-analysis using results from each individual GWAS using METAL. Variants reaching a suggestive threshold of association ($P \leq 1 \times 10^{-5}$) in the meta-analysis were then carried forward for downstream analyses, including

functional and colocalization analyses. Variants reaching the genome-wide significant threshold ($P \leq 5 \times 10^{-8}$) and exhibiting $\geq 80\%$ colocalization between two NPEs were followed up using existing methylation data to assess the association. All variants reaching genome-wide significance were considered associated with the respective NPE. We also report variants that reached a suggestive threshold ($P \leq 5 \times 10^{-7}$) or reached the lower suggestive threshold ($P \leq 1 \times 10^{-5}$) and were in a previously known disease-associated locus. GTEx, Genotype-Tissue Expression Project; QTL, quantitative trait locus; eQTL, expression QTL; sQTL, splicing QTL; mQTL, methylation QTL; AD, Alzheimer's disease.

with clinical LOAD, but ~20% of clinically diagnosed patients do not have ADNC, and >50% of those with ADNC have comorbid non-AD pathologies^{3,10}. For example, transactive response (TAR) DNA-binding protein 43-kDa (TDP-43) pathology was found in >50% of elderly autopsied individuals¹¹ in a community-based cohort study. Limbic-predominant age-related TDP-43 encephalopathy (LATE) is an amnesic dementia syndrome defined by a distinguishing pattern of LATE-neuropathological change (LATE-NC) characterized by TDP-43 proteinopathy that is most severe in the medial temporal lobes^{3,12,13}. Hippocampal sclerosis of aging is characterized by neuronal death, gliosis and atrophy of the hippocampus beyond normal ranges based on levels of ADNC, commonly co-occurs with LATE-NC, and is associated with severe cognitive impairment^{12,14}.

Cerebrovascular pathologies also contribute to cognitive decline and dementia and are prevalent among elderly autopsied research participants¹⁵. Cerebral amyloid angiopathy (CAA) is characterized by amyloid- β deposition in cerebral blood vessels¹⁶. CAA often co-occurs with ADNC but can independently contribute to cerebral injury^{15,16}. Infarcts of both grossly visible arteries and microscopically examined vessels (the latter referred to as microinfarcts) are also common contributors to cognitive decline^{15,17}. Cerebral large-vessel atherosclerosis and small-vessel/arteriolar thickening (arteriolosclerosis) are associated with infarcts, white matter rarefaction and hippocampal sclerosis^{18,19} and contribute to cognitive decline^{20,21}. Collectively, these factors reveal a complex web of pathologies that contribute to cognitive impairment and dementia.

Examining the genetic risk factors of each subtype of neuropathology can provide an important and complementary approach to large GWAS of clinical- and family history-based outcomes for studying LOAD/ADRD risk. Previous GWAS of NPEs have confirmed known LOAD risk loci and have identified new neuropathology risk loci²²⁻²⁷. Some NPEs, particularly LATE-NC, have yet to be studied systematically using GWAS. Here we performed GWAS on 11 NPEs using three high-quality data sources with both autopsy and genotype data. We also performed downstream functional analyses to explore potential biological functional mechanisms of newly identified risk loci and provide insight into previously identified putative AD risk loci.

Results

Participant and NPE characteristics

Genotype and neuropathology data were analyzed from the following three autopsy data sources: (1) the National Alzheimer's Coordinating Center (NACC; $n = 5,940$), (2) the Religious Orders Study and Rush Memory and Aging Project (ROSMAP; $n = 1,183$) and (3) the Adult Changes in Thought (ACT; $n = 681$) study (Fig. 1). In total, 7,804 unique participants were included in our analyses. The number of participants included in each GWAS ranged from 6,363 for amyloid- β plaques to 7,786 for Consortium to Establish a Registry for Alzheimer's Disease (CERAD) neuritic amyloid plaque score, except for LATE-NC, which had a smaller sample due to the more recent discovery and evaluation of TDP-43 pathology ($n = 3,112$; Table 1).

The 11 studied NPEs included AD-related pathologies (CERAD score for neuritic amyloid plaques, amyloid- β plaques including diffuse plaques and Braak NFT staging^{28–30}), non-AD neurodegenerative proteinopathies (LATE-NC and Lewy bodies^{12,31}), cerebrovascular pathologies (CAA, gross infarcts, microinfarcts, circle of Willis atherosclerosis and arteriolosclerosis^{30,32}) and hippocampal sclerosis³². NPEs commonly co-occurred, forming the following four identifiable clusters of pathologies: vascular, AD, LATE and Lewy body (Extended Data Fig. 1). Methods, Supplementary Methods and Supplementary Table 1 describe the applied phenotype definitions and harmonization approach.

GWAS meta-analysis of NPEs

We first performed GWAS on the 11 NPEs for the NACC, ROSMAP and ACT studies separately (Fig. 1). Genetic association analyses were performed with logistic or proportional-odds logistic regression mixed-effects models as appropriate (Methods). We then performed fixed-effects meta-analyses using METAL 2011-03-25 (ref. 33) on variants with minor allele frequencies $\geq 1\%$ in all studies³³. Quantile–quantile plots and corresponding estimates of genomic inflation (λ values) did not suggest systematic bias (Extended Data Fig. 2).

In total, the meta-analysis revealed seven loci with at least one variant meeting genome-wide significance ($P < 5 \times 10^{-8}$) across eight NPEs (amyloid- β plaques, arteriolosclerosis, atherosclerosis, Braak NFT stage, CAA, CERAD plaque score, hippocampal sclerosis and LATE-NC), with a total of 13 associations between genomic loci and NPEs (Fig. 2). Four of the seven loci were from genes previously associated with late-onset AD (the broader *APOE* region, *TMEM106B*, *GRN* and *BINI*; Fig. 2a–c,f,i,k), while three loci were new, where the lead variant was in or closest to *PIK3R5*, *LZTS1* and *COL4A1*, respectively (Fig. 2b,d,e). Although most meta-analyses had no significantly different effect size estimates across the three data sources, there were three with significant tests for heterogeneity (Table 2), all of which were associations with *APOE*.

We subsequently discovered a new locus near *APOC2* within the broader *APOE* region that is associated with CAA after adjusting for *APOE* ϵ diplotypes (Fig. 2f). No loci reached genome-wide significance with gross infarcts, microinfarcts or Lewy body pathology (Fig. 2g–j).

Known ADRD-associated loci. As expected, the *APOE* region (rs429358) is associated with multiple NPEs at genome-wide significance. Specifically, the *APOE* region (rs429358) is associated with (1) amyloid- β plaques (odds ratio (OR) = 1.98; $P = 2.3 \times 10^{-55}$; Table 2 and Fig. 2a), (2) Braak NFT stage (OR = 2.06, $P = 9.7 \times 10^{-89}$; Fig. 2b), (3) CERAD score (OR = 2.42, $P = 4.7 \times 10^{-103}$; Fig. 2c), (4) CAA (OR = 2.49, $P = 4.4 \times 10^{-138}$; Fig. 2f) and (5) LATE-NC (OR = 1.70, $P = 1.7 \times 10^{-14}$; Fig. 2i). Our results corroborate previous studies^{22,34} that described an association between *APOE* and CAA.

BINI was associated with Braak NFT stage (rs6733839; OR = 1.21; $P = 1.6 \times 10^{-9}$; Table 2 and Fig. 2b), and variants within *TMEM106B* were associated with both LATE-NC (rs2043539; OR = 0.70, $P = 5.8 \times 10^{-11}$; Fig. 2i) and hippocampal sclerosis (rs7805419; OR = 0.65; $P = 3.2 \times 10^{-13}$; Fig. 2k). A locus in *GRN* was also associated with hippocampal sclerosis (rs5848; OR = 1.40, $P = 3.2 \times 10^{-8}$; Fig. 2k).

New loci outside the *APOE* region. We also discovered three new loci outside the broader *APOE* region that are associated with three NPEs. Associations identified in the NPE GWAS meta-analysis included a *PIK3R5* intronic locus associated with Braak NFT stage (rs72844606; OR = 0.69, $P = 4.0 \times 10^{-8}$; Table 2 and Figs. 2b and 3a,b), an intronic *LZTS1* locus associated with arteriolosclerosis (rs78909048; OR = 0.44, $P = 5.7 \times 10^{-10}$; Figs. 2d and 3d,e) and a variant 12 kilobase pairs (kbp) upstream of *COL4A1* associated with the circle of Willis atherosclerosis (rs2000660; OR = 0.73, $P = 2.7 \times 10^{-8}$; Figs. 2e and 3g,h).

We next characterized which cell type(s) in the human brain express the new genes identified. According to brainrnaseq.org^{35,36}, *PIK3R5* is most highly expressed in microglia (Fig. 3c), *LZTS1* is most highly expressed in fetal astrocytes and endothelial cells (Fig. 3f) and *COL4A1* is most highly expressed in fetal astrocytes, endothelial cells and neurons (Fig. 3i).

New locus association within the *APOE* region. Based on the meta-analysis, we observed 12 genetic locus-phenotype associations within the broader *APOE* region (defined as less than 500 kbp from the start or end site of *APOE* transcription) across five NPEs (amyloid plaques, Braak stage, CAA, CERAD score and LATE-NC), where *APOE* itself (rs429358) was the top variant in the region for all five NPEs (Fig. 2a–c,f,i). We performed additional analyses in this region adjusting for *APOE* ϵ diplotypes to determine whether any of the genome-wide significant signals within the broader *APOE* region remained significant.

In the *APOE*-adjusted analysis, the lead variant from the non-adjusted analysis (rs429358), which tags the *APOE* $\epsilon 4$ allele (the well-known common variant with the strongest association with LOAD), was no longer associated with any of the five phenotypes. One locus with lead variant rs7247551 remained significantly associated with CAA (OR = 0.81; $P = 8.0 \times 10^{-12}$; Table 2 and Fig. 2f). rs7247551 is located between *APOC2* and *CLPTM1*. No variants remained genome-wide significantly associated with any other *APOE*-associated NPE. Sensitivity analyses showed that the effect size of rs7247551 did not significantly differ based on *APOE* diplotype in NACC, ROSMAP or ACT (Supplementary Results and Extended Data Fig. 3).

***APOC2* replicates in an independent cohort.** We obtained data from a recent GWAS of CAA in 815 participants with dementia in the Mayo Clinic Brain Bank. Using their data, we replicated the association between rs7247551 and CAA while adjusting for *APOE* ϵ diplotypes ($P = 0.0012$). We also confirmed that rs7247551 was indeed new and not in linkage disequilibrium (LD) with the variant previously reported in ref. 26 (rs5117; $r^2 < 0.01$). Together, these results provide evidence for a new locus within the broader *APOE* region that is independent of the *APOE* ϵ diplotypes and is associated with CAA pathology burden. It further suggests that the genetic risk for CAA in the broader *APOE* region may differ from the AD-specific neuropathologies (neuritic amyloid plaques and NFT).

Associations of clinical and proxy AD risk loci with NPE

We further tested whether LOAD-associated loci identified in a recent AD (hereafter, 'ADRD') GWAS were associated with any evaluated NPEs⁶. Reference 6 identified a total of 83 distinct non-*APOE* loci (39 previously identified and 44 new) associated with AD (hereafter, 'ADRD loci'), 77 of which had lead variants that met inclusion criteria in our study. In total, 23 NPE-locus associations from 19 loci had adjusted P (Q values) ≤ 0.05 across the 11 NPEs. In total, 13 of these 19 loci were not already reported herein. Of the 23 associations, 22 had concordant directions of effect with ref. 6 (Table 3 and Supplementary Table 2).

Notably, the pathognomonic AD pathologies, operationalized using Braak NFT stage and CERAD score, had concordant directions of effect with 70 and 60 of the 77 ADRD loci, respectively, regardless of statistical significance. Three ADRD loci (*BINI*, *MME* and *HLA-DQA1*; Table 3) were significantly associated with the Braak NFT stage after multiple testing corrections. Two ADRD loci (*PICALM* and *TPCNI*) were associated with CAA. Ten ADRD loci (*CR1*, *BINI*, *INPP5D*, *ZCWPW1/NYAP1*, *PTK2B*, *PICALM*, *SORL1*, *FERMT2*, *SNX1* and *ABCA7*) were significantly associated with the CERAD score after multiple testing corrections. Four ADRD loci (*TMEM106B*, *IL34*, *GRN* and *MAPT*) were significantly associated with hippocampal sclerosis, all of which except for *IL34* (hippocampal sclerosis—OR = 0.74, $P = 0.0019$; AD—OR = 1.06, $P = 5.6 \times 10^{-6}$) were concordant in effect direction. Two ADRD loci (*TMEM106B* and

Table 1 | Demographic and pathology characteristics of the NACC, ROSMAP, ACT cohorts and combined sample

Characteristics ^a	NACC (n=5,940)	ROSMAP (n=1,183)	ACT (n=681)	Overall (n=7,804)	P value ^b
Sex					
Female	2,980 (50.2%)	798 (67.5%)	381 (55.9%)	4,159 (53.3%)	<0.001
Male	2,960 (49.8%)	385 (32.5%)	300 (44.1%)	3,645 (46.7%)	
Age of death (year)					
Mean (s.d.)	81.4 (9.81)	89.6 (6.48)	88.6 (6.61)	83.3 (9.73)	<0.001
Median (minimum and maximum)	82 (39, 111)	90 (66, 108)	89 (70, 106)	84 (39, 111)	
AD					
Not impaired	634 (10.7%)	363 (30.7%)	594 (87.2%)	1,591 (20.4%)	<0.001
AD/MCI	4,605 (77.5%)	776 (65.6%)	68 (10.0%)	5,449 (69.8%)	
Unknown/other dementia	701 (11.8%)	44 (3.7%)	19 (2.8%)	764 (9.8%)	
Dementia					
No dementia	1,029 (17.3%)	649 (54.9%)	594 (87.2%)	2,272 (29.1%)	<0.001
Dementia	4,911 (82.7%)	511 (43.2%)	87 (12.8%)	5,509 (70.6%)	
Missing	0 (0%)	23 (1.9%)	0 (0%)	23 (0.3%)	
APOE ε4 alleles					
0	2,710 (45.6%)	883 (74.6%)	489 (71.8%)	4,082 (52.3%)	<0.001
1	2,547 (42.9%)	280 (23.7%)	174 (25.6%)	3,001 (38.5%)	
2	680 (11.4%)	20 (1.7%)	15 (2.2%)	715 (9.2%)	
Missing	3 (0.1%)	0 (0%)	3 (0.4%)	6 (0.1%)	
AD-related NPEs					
Amyloid-β plaques					
None	407 (6.9%)	222 (18.8%)	64 (9.4%)	693 (8.9%)	<0.001
Mild	515 (8.7%)	351 (29.7%)	34 (5.0%)	900 (11.5%)	
Moderate	884 (14.9%)	278 (23.5%)	71 (10.4%)	1,233 (15.8%)	
Severe	3,079 (51.8%)	317 (26.8%)	141 (20.7%)	3,537 (45.3%)	
Missing	1,055 (17.8%)	15 (1.3%)	371 (54.5%)	1,441 (18.5%)	
Braak NFT stage					
0	79 (1.3%)	12 (1.0%)	19 (2.8%)	110 (1.4%)	<0.001
1	211 (3.6%)	75 (6.3%)	56 (8.2%)	342 (4.4%)	
2	365 (6.1%)	109 (9.2%)	111 (16.3%)	585 (7.5%)	
3	490 (8.2%)	281 (23.8%)	125 (18.4%)	896 (11.5%)	
4	860 (14.5%)	370 (31.3%)	130 (19.1%)	1,360 (17.4%)	
5	1,491 (25.1%)	307 (26.0%)	149 (21.9%)	1,947 (24.9%)	
6	2,431 (40.9%)	18 (1.5%)	87 (12.8%)	2,536 (32.5%)	
Missing	13 (0.2%)	11 (0.9%)	4 (0.6%)	28 (0.4%)	
CERAD score					
None	578 (9.7%)	279 (23.6%)	155 (22.8%)	1,012 (13.0%)	<0.001
Mild	509 (8.6%)	103 (8.7%)	174 (25.6%)	786 (10.1%)	
Moderate	1,071 (18.0%)	399 (33.7%)	169 (24.8%)	1,639 (21.0%)	
Severe	3,777 (63.6%)	391 (33.1%)	181 (26.6%)	4,349 (55.7%)	
Missing	5 (0.1%)	11 (0.9%)	2 (0.3%)	18 (0.2%)	
Cerebrovascular NPEs					
Arteriolosclerosis					
None	1,231 (20.7%)	407 (34.4%)	7 (1.0%)	1,645 (21.1%)	<0.001
Mild	1,577 (26.5%)	398 (33.6%)	147 (21.6%)	2,122 (27.2%)	
Moderate	1,501 (25.3%)	277 (23.4%)	289 (42.4%)	2,067 (26.5%)	
Severe	621 (10.5%)	81 (6.8%)	132 (19.4%)	834 (10.7%)	
Missing	1,010 (17.0%)	20 (1.7%)	106 (15.6%)	1,136 (14.6%)	

Table 1 (continued) | Demographic and pathology characteristics of the NACC, ROSMAP, ACT cohorts and combined sample

Characteristics ^a	NACC (n=5,940)	ROSMAP (n=1,183)	ACT (n=681)	Overall (n=7,804)	P value ^b
Atherosclerosis					
None	1,251 (21.1%)	221 (18.7%)	33 (4.8%)	1,505 (19.3%)	
Mild	2,027 (34.1%)	577 (48.8%)	182 (26.7%)	2,786 (35.7%)	
Moderate	1,507 (25.4%)	317 (26.8%)	407 (59.8%)	2,231 (28.6%)	<0.001
Severe	711 (12.0%)	60 (5.1%)	47 (6.9%)	818 (10.5%)	
Missing	444 (7.5%)	8 (0.7%)	12 (1.8%)	464 (5.9%)	
CAA					
None	1,928 (32.5%)	253 (21.4%)	414 (60.8%)	2,595 (33.3%)	
Mild	1,603 (27.0%)	482 (40.7%)	124 (18.2%)	2,209 (28.3%)	
Moderate	1,327 (22.3%)	261 (22.1%)	121 (17.8%)	1,709 (21.9%)	<0.001
Severe	707 (11.9%)	141 (11.9%)	20 (2.9%)	868 (11.1%)	
Missing	375 (6.3%)	46 (3.9%)	2 (0.3%)	423 (5.4%)	
Gross infarcts					
Absent	4,402 (74.1%)	753 (63.7%)	477 (70.0%)	5,632 (72.2%)	
Present	1,146 (19.3%)	416 (35.2%)	204 (30.0%)	1,766 (22.6%)	<0.001
Missing	392 (6.6%)	14 (1.2%)	0 (0%)	406 (5.2%)	
Microinfarcts					
Absent	4,475 (75.3%)	820 (69.3%)	346 (50.8%)	5,641 (72.3%)	
Present	1,160 (19.5%)	349 (29.5%)	330 (48.5%)	1,839 (23.6%)	<0.001
Missing	305 (5.1%)	14 (1.2%)	5 (0.7%)	324 (4.2%)	
Non-AD NPEs					
LATE-NC					
None	921 (15.5%)	509 (43.0%)	357 (52.4%)	1,787 (22.9%)	
Mild	75 (1.3%)	194 (16.4%)	147 (21.6%)	416 (5.3%)	
Moderate	317 (5.3%)	117 (9.9%)	149 (21.9%)	583 (7.5%)	<0.001
Severe	50 (0.8%)	267 (22.6%)	9 (1.3%)	326 (4.2%)	
Missing	4,577 (77.1%)	96 (8.1%)	19 (2.8%)	4,692 (60.1%)	
Lewy body					
None	3,749 (63.1%)	861 (72.8%)	539 (79.1%)	5,149 (66.0%)	
Mild	199 (3.4%)	23 (1.9%)	20 (2.9%)	242 (3.1%)	
Moderate	732 (12.3%)	92 (7.8%)	60 (8.8%)	884 (11.3%)	<0.001
Severe	726 (12.2%)	157 (13.3%)	60 (8.8%)	943 (12.1%)	
Missing	534 (9.0%)	50 (4.2%)	2 (0.3%)	586 (7.5%)	
Hippocampal sclerosis					
Absent	4,777 (80.4%)	1,053 (89.0%)	583 (85.6%)	6,413 (82.2%)	
Present	572 (9.6%)	100 (8.5%)	79 (11.6%)	751 (9.6%)	0.056
Missing	591 (9.9%)	30 (2.5%)	19 (2.8%)	640 (8.2%)	

Cohort demographics—NACC participants had a higher percentage of patients diagnosed with mild cognitive impairment (MCI) or AD (78%) than ROSMAP (66%) or ACT (10%). NACC participants died at a younger age (mean age at death=81 years) compared to ROSMAP (90 years) and ACT (89 years) participants and had more balanced participation between the sexes, with 50% of NACC participants being female versus 68% and 58% in ROSMAP and ACT, respectively. NACC participants were also more likely to carry an APOE ε4 allele (54%) versus ROSMAP (25%) or ACT (28%; chi-square test, $P<0.001$ for all mentioned comparisons; the only not significant test was hippocampal sclerosis with $P=0.056$). Notably, NACC is based on data collected from over 30 ADRCs, which often recruit from clinic patients and their families. In contrast, the other studies recruited older persons without known dementia; ACT from the Seattle, WA area; ROS from members of the Catholic Church clergy; and MAP from northeastern Illinois. MCI, mild cognitive impairment. ^aExcept for the age of death, all distribution data are given as *n* and percentage. ^bExcept for the age of death (ANOVA), the *P* value from the chi-square test.

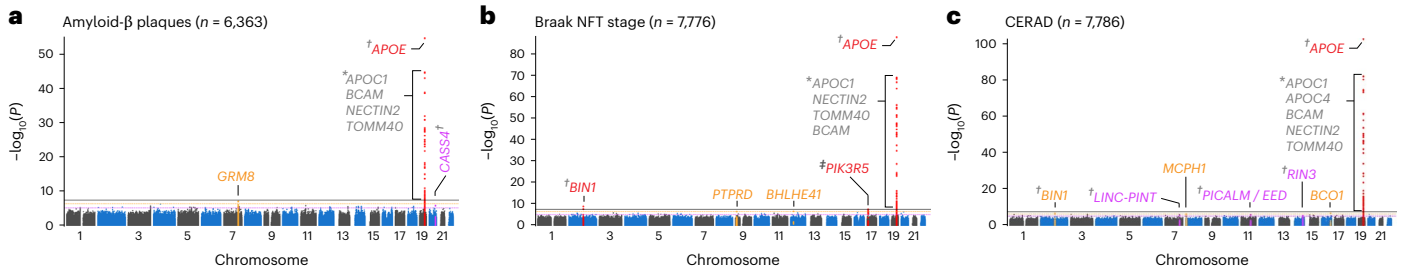
GRN were significantly associated with LATE-NC. Finally, two ADRC loci (*TPCNI* and *PLCG2*) were significantly associated with microinfarcts. These results indicate that NPE studies largely corroborate the findings of large AD GWAS based on clinical and proxy phenotypes. Several ADRC loci, particularly *MAPT* (hippocampal sclerosis), *TMEM106B* and *GRN* (hippocampal sclerosis and LATE-NC), were associated only with non-AD pathology.

Identifying potential genetic mechanisms of NPE development

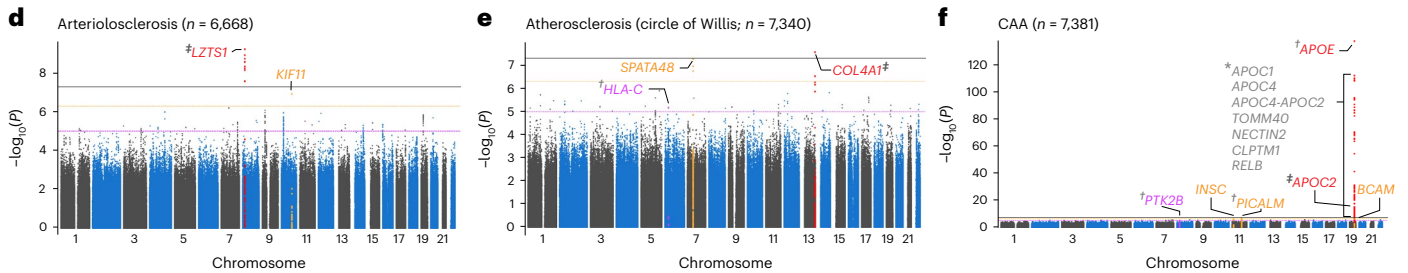
We also assessed possible mechanisms through which identified NPE-associated variants may be involved in disease risk.

Gene-prioritization and enrichment analyses. Using gene-based, pathway, and enrichment analyses, we identified *APOE* as significantly

AD-related NPEs

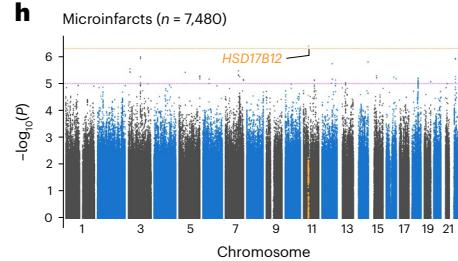
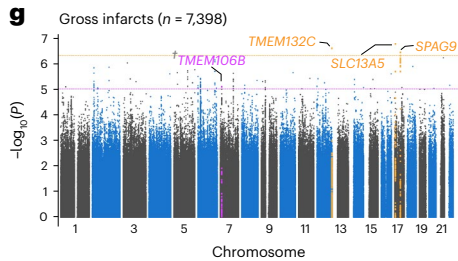


Cerebrovascular NPEs



Known disease loci

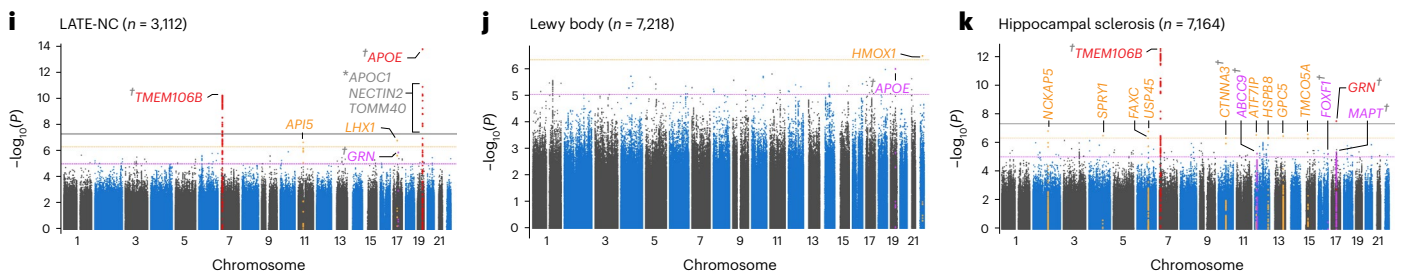
- Genome-wide sig. (9 assoc.; red):
1. APOE (5 assoc.)
 2. BIN1 (Braak)
 3. GRN (HS)
 4. TMEM106B (HS; LATE-NC)
- Sugg. ($P < 5 \times 10^{-7}$; 3 assoc.; gold):
1. BIN1 (CERAD)
 2. CTNNA3 (HS)
 3. PICALM/EED (CAA)
- Sugg. ($P < 1 \times 10^{-5}$; 12 assoc.; purple):
1. ABCG9 (HS)
 2. APOE (Lewy body)
 3. CASS4 (A β plaques)
 4. FOXF1 (HS)
 5. GRN (LATE-NC)
 6. HLA-C (atherosclerosis)
 7. LINC-PINT (CERAD)
 8. MAPT (HS)
 9. PICALM/EED (CERAD)
 10. PTK2B (CAA)
 11. RIN3 (CERAD)
 12. TMEM106B (gross infarcts)



New disease loci

- Genome-wide sig. (4 assoc.; red):
1. PIK3R5 (Braak NFT stage)
 2. LZTS1 (arteriolosclerosis)
 3. COL4A1 (atherosclerosis)
 4. APOC2 (CAA)
- Sugg. ($P < 5 \times 10^{-7}$; 24 assoc.; gold): see Supplementary Table 2

Non-AD NPEs



- Genome-wide sig. ($P < 5 \times 10^{-8}$)
- Near genome-wide sig. ($P < 5 \times 10^{-7}$)
- Suggestive sig. ($P < 1 \times 10^{-5}$) and putative disease gene from previous studies

- * Putative new disease gene identified herein
- † Putative disease gene from previous studies

- * Genome-wide significant hits within broader APOE region that did not survive conditional analysis

Fig. 2 | Manhattan plots identify loci associated with each of the 11 NPEs included in this study. a–k. Manhattan plots are shown for amyloid- β plaques (a), Braak NFT stage (b), CERAD score for neuritic plaques (c), arteriolosclerosis (d), atherosclerosis in the circle of Willis (e), CAA (f), gross infarcts (g), microinfarcts (h), LATE-NC (i), Lewy body (j) and hippocampal sclerosis (k). The y axes denote the $-\log_{10}(P)$ value of meta-analysis two-sided z test) of the variant-phenotype association, and the x axes outline the chromosomal position, with alternate chromosomes represented in black and blue. Labels indicate the nearest gene at a locus. The horizontal lines define the genome-wide significance level (solid black, $P = 5 \times 10^{-8}$), near genome-wide significance level (dotted gold, $P = 5 \times 10^{-7}$), and suggestive significance level ($P < 5 \times 10^{-5}$) in loci with evidence of AD association from a previous study (for example, ref. 6; dotted purple). Points and gene symbols are coded with the same colors. Gray gene symbols indicate genome-wide significant hits within the APOE region that did not survive conditional analysis. All GWAS are in cohorts of European ancestry and adjusted for age at death, sex, genotyping cohort and top ten genetic PCs. We identified

eight genome-wide significant loci and 39 near genome-wide significant or suggestive loci. The genome-wide significant loci resulted in 14 associations with eight NPEs (amyloid- β plaques, arteriolosclerosis, atherosclerosis, Braak NFT stage, CAA, CERAD score, hippocampal sclerosis and LATE-NC). Four genes were previously associated with AD (APOE, BIN1, TMEM106B, GRN; a–c, f, i, k), while the four new loci were in or closest to PIK3R5, LZTS1, COL4A1 and APOC2 (b, d, e, f). APOC2 is within the broader APOE region but remained significantly associated with CAA after adjusting for APOE ϵ diplotypes (f). Three NPEs (gross infarcts, microinfarcts and Lewy bodies) had zero genome-wide significant hits, but all three had near genome-wide significant and/or suggestive hits from either new or known loci. APOE was associated with a range of NPEs, including LATE-NC, which is not pathognomonic of AD. On the other hand, neither GRN nor TMEM106B (recently identified in AD GWAS) was associated with the AD pathognomonic NPEs but were specific to gross infarcts, LATE-NC and hippocampal sclerosis at either genome-wide or suggestive significance. sig., significant; assoc., associations; sugg., suggestive.

Table 2 | Significant NPE-associated loci in GWAS meta-analysis of NACC, ROSMAP and ACT datasets

Phenotype	Gene ^a	Variant	Chr	Position ^b	Min/maj	OR ^c (95% CI)	P value	Het. P value ^d
Braak NFT stage	<i>BIN1</i>	rs6733839	2	127,135,234	T/C	1.21 (1.14–1.29)	1.6×10 ⁻⁹	0.054
LATE-NC	<i>TMEM106B</i>	rs2043539	7	12,214,254	A/G	0.70 (0.63–0.78)	5.8×10 ⁻¹¹	0.37
Hippocampal sclerosis	<i>TMEM106B</i>	rs7805419	7	12,242,825	C/T	0.65 (0.58–0.73)	3.2×10 ⁻¹³	0.25
Arteriosclerosis	LZTS1	rs78909048	8	20,279,428	G/A	0.44 (0.34–0.57)	5.7×10⁻¹⁰	0.85
Atherosclerosis	COL4A1	rs2000660	13	110,136,094	A/G	0.73 (0.66–0.82)	2.7×10^{-8e}	0.85
Braak NFT stage	PIK3R5	rs72844606	17	8,930,274	T/C	0.69 (0.60–0.79)	4.0×10^{-8e}	0.27
Hippocampal sclerosis	<i>GRN</i>	rs5848	17	44,352,876	T/C	1.40 (1.24–1.57)	3.2×10 ^{-8e}	0.48
Braak NFT stage	<i>APOE</i>	rs429358	19	44,908,684	C/T	2.06 (1.92–2.21)	9.7×10 ⁻⁸⁹	6.6×10 ⁻⁵
CAA	<i>APOE</i>	rs429358	19	44,908,684	C/T	2.49 (2.32–2.67)	4.4×10 ⁻¹³⁸	4.2×10 ⁻⁴
CERAD score	<i>APOE</i>	rs429358	19	44,908,684	C/T	2.42 (2.23–2.62)	4.7×10 ⁻¹⁰³	0.14
LATE-NC	<i>APOE</i>	rs429358	19	44,908,684	C/T	1.70 (1.48–1.95)	1.7×10 ⁻¹⁴	0.28
Amyloid-β plaques	<i>APOE</i>	rs429358	19	44,908,684	C/T	1.98 (1.82–2.16)	2.3×10 ⁻⁵⁵	6.6×10 ⁻⁴
CAA ^f	APOC2	rs7247551	19	44,951,509	G/A	0.81 (0.76–0.86)	8.0×10⁻¹²	0.42

Bold text indicates loci not previously associated with ADRD. CI, confidence interval; Min/maj, minor allele/major allele; Het., heterogeneity. ^aClosest protein-coding gene according to GENCODE release 40. ^bGenome positions are based on build HG38. ^cORs are with respect to minor alleles. ^dP value from the test for effect size heterogeneity across data sources. ^eReaches genome-wide significance within the single NPE but does not reach experiment-wide significance when adjusting for 11 NPEs ($P = \frac{5 \times 10^{-8}}{11} = 4.55 \times 10^{-9}$). ^fResult from *APOE* diplotype-adjusted analysis.

associated with NFT, diffuse plaques, CAA, neuritic plaques and LATE-NC (Supplementary Table 3)³⁷. *TMEM106B* was associated with both hippocampal sclerosis and LATE-NC. We further found that rs2000660 (associated with the circle of Willis atherosclerosis) is located within an enhancer region 13 kbp upstream of *COL4A1* transcription start site (Extended Data Fig. 4). Annotations from FAVOR identified a synonymous, exonic single-nucleotide polymorphism (SNP), rs650724, in high LD ($r^2 = 0.86$) with this lead variant that is highly conserved across mammals (mamPhCons = 0.987; Supplementary Table 4)³⁸.

Genetic colocalization analysis. We investigated whether loci associated with multiple NPEs show evidence for genetic colocalization³⁹. We identified two NPE pairs exhibiting genetic colocalization, including (1) Braak NFT stage and CERAD score (*BIN1*; probability of colocalization (PrC) > 99%; Extended Data Fig. 5) and (2) hippocampal sclerosis and LATE-NC (*TMEM106B*; PrC > 90%; Fig. 4a–c).

We also tested for colocalization between NPE loci and quantitative trait loci (QTL). The *TMEM106B* locus (associated with hippocampal sclerosis and LATE-NC) colocalized with *TMEM106B* expression in multiple tissues, including the cerebellar hemisphere (PrC = 90%; Fig. 4d,e). Two CpG sites located either within *TMEM106B* (cg09613507; Fig. 4f) or upstream (cg23422036; Fig. 4h) colocalized with both hippocampal sclerosis (cg09613507-hippocampal sclerosis PrC = 94%, cg23422036-hippocampal sclerosis PrC = 94%; Fig. 4b,f,g) and LATE-NC (cg09613507-LATE-NC PrC = 89% and cg23422036-LATE-NC PrC = 95%; Fig. 4a,f–i). A hippocampal sclerosis-associated locus within *GRN* strongly colocalized with both LATE-NC and *GRN* expression in multiple tissues (PrC > 99.9%; Extended Data Fig. 6).

APOC2 colocalized with several traits, including methylation QTL (mQTL) for four CpG sites in ROSMAP (cg04401876, cg10169327, cg13119609 and cg09555818; PrC = 96–99%; Fig. 5a–i). The *APOC2* locus also colocalized with an expression of multiple genes in Genotype-Tissue Expression Project (GTEx), including *APOE* expression in the wall of the aorta (PrC = 94%), *CLPTM1* expression in the skin of the leg and suprapubic region and *APOC2* expression in 14 different tissues (for example, brain cortex, caudate, nucleus accumbens and cerebellum; PrC = 90–97%).

Multiple suggestive NPE loci showed evidence of colocalization with expression QTL (eQTL) in GTEx. In total, 44 NPE loci (lead variant $P < 1 \times 10^{-5}$) colocalized with various QTL types (that is, expression,

methylation or splicing QTL [sQTL]; PrC ≥ 80%). A total of 550 NPE–QTL pairs colocalized across 44 tissues (Supplementary Table 5), many giving credence to previously discovered associations and insight into potential mechanisms. For example, rs1643235 (*ABCC9*) colocalized with hippocampal sclerosis and gene expression in multiple tissues, including the cortex (PrC = 80%), corroborating previous studies^{27,40,41} because the *ABCC9* SNP rs4148674 ($r^2 = 0.96$ with rs1643235) was a robust eQTL for *ABCC9* and the strongest *ABCC9* region signal for association with hippocampal sclerosis (Extended Data Fig. 7).

Functional studies in ROSMAP. Using data from ROSMAP participants with DNA methylation and/or RNA-sequencing (RNA-seq) data available from the dorsolateral prefrontal cortex (DLPFC), we found that neither *TMEM106B* nor *GRN* expression was associated with hippocampal sclerosis ($P > 0.05$), while decreased *TMEM106B* expression was associated with more severe LATE-NC pathology ($P = 0.043$; Fig. 4j). Of the two CpG sites that colocalized with hippocampal sclerosis and LATE-NC, hypermethylation of cg09613507 was associated with more severe LATE-NC pathology ($P = 0.0093$; Fig. 4k), while cg23422036 was not significantly associated ($P = 0.10$; Fig. 4l).

Additionally, we tested for association between CAA pathology and methylation levels at four CpG sites (cg09555818, cg04401876, cg10169327 and cg13119609) that colocalized with the chromosome 19 (chr19) CAA risk locus (rs7247551). We first confirmed that all four CpG sites were significantly associated with rs7247551 ($P < 0.0001$) and had directions of effect consistent with those previously reported for ROSMAP⁴². Hypomethylation at cg09555818 (OR = 0.82, $P = 0.003$) and cg13119609 (OR = 0.78, $P = 0.0006$) were significantly associated with more severe CAA pathology (Fig. 5j). Both cg09555818 ($P = 0.0063$; Fig. 5k) and cg13119609 ($P = 0.0069$) were significantly associated with *APOC2* expression.

Next, as *APOC2* expression in multiple brain tissues colocalized with CAA in GTEx but not ROSMAP, we investigated whether there was a nominal association between *APOC2* expression in the DLPFC and rs7247551. We found that the G allele of rs7247551 was nominally associated with increased *APOC2* expression in the DLPFC ($\beta = 0.072$, $P = 0.00013$; Fig. 5l); however, the direction of effect was opposite of that found in brain tissues in GTEx (that is, the G allele of rs7247551 was associated with decreased *APOC2* expression in GTEx; $P = 7.2 \times 10^{-7}$; Fig. 5m). Expression of *APOC2* in the DLPFC was not associated with CAA in ROSMAP (OR = 0.98, $P = 0.89$). We performed an additional post hoc

analysis for nominal *APOE* eQTL activity of *rs7247551* in ROSMAP. We confirmed that *rs7247551* was not associated with *APOE* expression in the DLPCF in ROSMAP ($P = 0.81$; Fig. 5n). *APOC2* expression was also not significantly associated with the severity of CAA pathology in ROSMAP ($P = 0.089$; Fig. 5o). Notably, *APOC2* is highly expressed, especially in microglia and oligodendrocytes (Fig. 5p).

Potential effects via differential RNA splicing. Many human genes undergo alternative splicing^{43–45}. Recent work in ref. 46 demonstrated that many medically relevant genes express multiple RNA isoforms that result in unique proteins, including genes involved in ADRD. Specific examples include *APP*, *MAPT* and *BINI*, which express five, five and eight distinct RNA isoforms above noise levels, respectively, in the human frontal cortex. Thus, we explored whether any genes associated with NPEs in this work express multiple RNA isoforms in the human frontal cortex.

While all loci that were associated with NPE have multiple annotated RNA isoforms, ranging from 4 (*LZTS1*) to 24 (*PICALM*) per Ensembl, most of the genes exhibited expression for only a single isoform above noise levels, per data from ref. 46. Some expressed multiple RNA isoforms, but the isoforms were not predicted to result in distinct proteins (for example, *LZTS1*)—although recent data suggest that alternative untranslated regions have direct functional consequences^{47–49}. *BINI*, however, actively transcribes eight distinct RNA isoforms in the frontal cortex (Fig. 4m). *BINI* is also expressed in multiple brain cell types in humans, according to brainrnaseq.org^{35,36}. Given the diversity of *BINI* isoforms simultaneously expressed, we need to understand whether specific isoforms are involved in disease, and we propose differential RNA isoform expression as a potential mechanism through which disease genes may be affecting disease.

Discussion

The present study of 11 ADRD-related NPEs comprised 7,804 participants. These results provide an autopsy-based complement to previous studies based on clinical diagnoses and expand on the findings of previous genetic studies of dementias and neuropathologies^{2,6,22–24,26,41}. In this work, we confirm previous findings that several loci associated with AD (including *APOE*) are also associated with non-ADNC pathogenesis. Additionally, some of the known ADRD loci (that is, *TMEM106B* and *GRN*) did not associate with any of the classical AD-defining NPEs in this study. Thus, our results improve our collective understanding of the complex nature of ADRD and its genetic bases.

Sharpening the endophenotypes enabled the discovery of new hit genes that did not reach genome-wide significance in previous studies oriented toward studying AD clinical phenotypes. We identified clear genetic associations between specific neuropathologies and loci already associated with ADRD and four new NPE-associated loci.

Yet, many questions remain and will require deeper investigation. For example, three of the NPEs studied (gross infarcts, microinfarcts and Lewy body pathology) did not have any locus reach genome-wide significance in our study. Likely explanations for the lack of genome-wide associations for these three pathologies include (1) insufficient sample size, (2) the cohorts not being specifically designed to study these phenotypes, and (3) variability in the collection and scoring of these phenotypes over time and between research centers. Nonetheless, these three NPEs each had suggestive associations, including with known loci (Supplementary Results). Specifically, *TMEM106B* and *APOE* had suggestive associations with gross infarcts and Lewy body pathology, respectively. *APOE* $\epsilon 4$ was previously associated with Lewy body pathology by a study discussed in ref. 50. As study cohorts grow larger, researchers will be able to re-assess these suggestive associations.

As expected, *APOE* variation was associated with ADNC, CAA and LATE-NC. Although LATE-NC is diagnostically characterized by TDP-43 proteinopathy^{3,12,13}, brains with a greater burden of neuritic amyloid plaques are more likely to have TDP-43 proteinopathy (and vice versa)¹². Similarly, others have previously shown an association between *APOE* $\epsilon 4$ status and TDP-43 pathology in ROSMAP¹¹. Unraveling the complex interaction between *APOE* and proteinopathies (including the suggestive association to Lewy bodies) may provide a crucial insight into properly treating patients with these often comorbid pathologies. A study using a mouse model suggests that TDP-43 directly interacts with amyloid- β and promotes worse pathology⁵¹, but further studies are needed to better understand this interaction.

By adjusting for *APOE* e diplotypes, we identified a new locus near *APOC2* associated with CAA. Like *APOE*, *APOC2* is part of the apolipoprotein family and is involved in lipoprotein metabolism. Both genes directly bind fat droplets (chylomicrons)^{52,53} and are implicated in heart disease⁵⁴—a known link to *APOE* and dementia. *APOC2* and *APOE* expression is also coregulated through the same mechanisms in liver^{52,53}. We replicated the association between *APOC2* and CAA while adjusting for *APOE* in an independent sample of 815 Mayo Clinic Brain Bank participants used in ref. 26, providing additional evidence for the *APOC2* locus being important for CAA pathology beyond the known effects of *APOE* e haplotypes.

Previously, a study discussed in ref. 55 reported that a variant proximal to *rs7247551* (*rs10413089*; 822 bp away) showed evidence of association with clinical AD independently of *APOE* e status in their cohort but determined their results were inconclusive. Their original association did not survive multiple testing corrections, but the association replicated in an independent cohort. Summary statistics from ref. 6 reflect that *rs7247551* was significantly associated with ADRD but did not report results of an independent analysis within the broader *APOE* region. Thus, the present study is the first to confirm that this

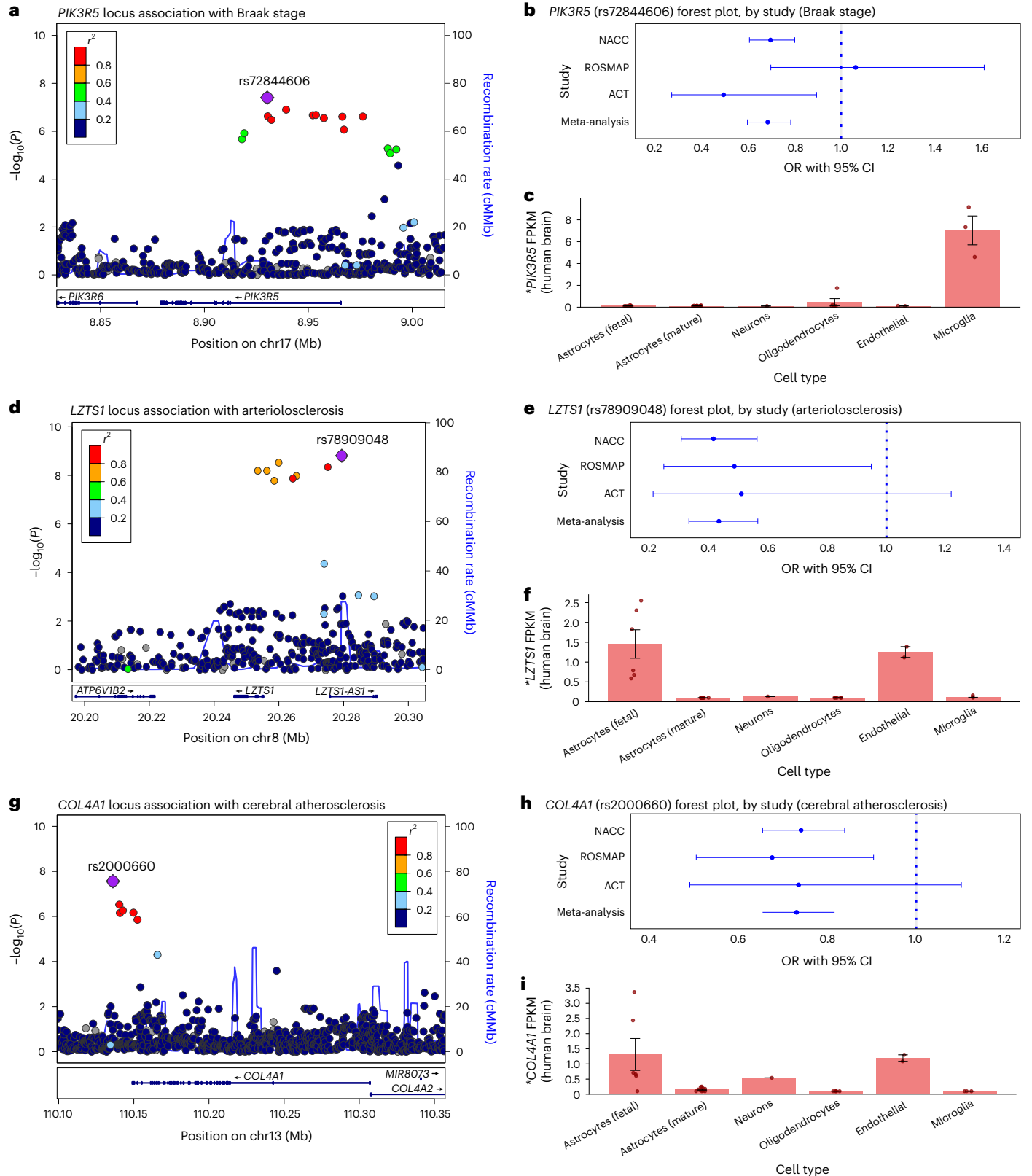
Fig. 3 | New associations identified between *PIK3RS*, *LZTS1* and *COL4A1* and Braak NFT stage, arteriolosclerosis and cerebral atherosclerosis, respectively. **a**, Braak stage association plot from NPE GWAS meta-analysis ($n = 7,776$) for the region around *PIK3RS*. Colored dots represent the chromosomal position (x axis, Mb) in hg38 coordinates and $-\log_{10}(P$ value from meta-analysis two-sided z test; y axis) of each variant in the region. Dots are colored to represent the LD r^2 with the lead variant (purple diamond) estimated with PLINK- $r2$ using 1000 Genomes phase 3 European-descended participants. The recombination rate was calculated using GRCh38 genetic map files downloaded from https://bochet.gcc.biostat.washington.edu/beagle/genetic_maps/ and taking the ratio of difference of CM and Mb between positions. Boxes below data indicate the location of genes in the region. (Plot generated using LocusZoom⁷³). **b**, Association of *PIK3RS* lead variant (*rs72844606*) with Braak stage for individual cohorts (NACC, $n = 5,927$; ROSMAP, $n = 1,172$ and ACT, $n = 677$) and meta-analysis ($n = 7,776$) using METAL (y axis). Points along the x axis represent OR of association, and error bars indicate 95% CI. **c**, Human brain cell-type expression profile of *PIK3RS* in ref. 35. Columns represent mean FPKM. Error bars indicate the s.e. of measurement for each cell

type based on the number of human samples sequenced for each type (fetal astrocytes, $n = 6$; mature astrocytes, $n = 12$; endothelial, $n = 2$; microglia, $n = 3$; neurons, $n = 1$ and oligodendrocytes, $n = 5$). *PIK3RS* is primarily expressed in microglia. **d**, Arteriolosclerosis association plot from NPE GWAS meta-analysis ($n = 6,668$) for the region around *LZTS1* (see **a** for interpretation). **e**, Association of *LZTS1* lead variant (*rs78909048*) with arteriolosclerosis for individual cohorts (NACC, $n = 4,930$; ROSMAP, $n = 1,163$ and ACT, $n = 575$) and meta-analysis ($n = 6,668$) using METAL (y axis; see **b** for interpretation). **f**, Human brain cell-type expression profile of *LZTS1* in ref. 35. *LZTS1* is primarily expressed in fetal astrocytes and endothelial cells (see **c** for interpretation). **g**, Cerebral atherosclerosis association plot from NPE GWAS meta-analysis ($n = 7,340$) for the region around *COL4A1* (see **a** for interpretation). **h**, Association of *COL4A1* lead variant (*rs2000660*) with cerebral atherosclerosis for individual cohorts (NACC, $n = 5,496$; ROSMAP, $n = 1,175$ and ACT, $n = 669$) and meta-analysis ($n = 7,340$) using METAL (y axis; see **b** for interpretation). **i**, Human brain cell-type expression profile of *COL4A1* in ref. 35. *COL4A1* is preferentially expressed in fetal astrocytes and endothelial cells with lower expression in neurons (see **c** for interpretation). Mb, megabase.

association is independent of the known effects of *APOE* alleles. Both the potential association with clinical AD status found by ref. 55 and the association with CAA we report herein should be followed up in future studies.

Several variants in the *APOC2* locus were lead eQTLs for *APOC2* brain expression in both GTEx and ROSMAP. Colocalization analysis

confirmed that the new CAA risk locus shares a functional variant with both *APOC2* eQTL and nearby brain cortex mQTL. We confirmed that two of the CpG sites affected by the CAA risk locus, cg09555818 and cg13119609, were, in turn, significantly associated with CAA pathology. Both CpG sites are located within the *APOC4*–*APOC2* readthrough transcript region, overlapping *APOC4* and *APOC2*. Our results are consistent



*Expression in human brain cells per brainrnaseq.org (ref. 35)

Table 3 | Associations between NPEs (using NACC, ROSMAP and ACT datasets) and known ADRD loci

NPE/ Chr	Locus ^a	Position ^b	Variant	Effect/ other allele	EAF ^c	NPE OR ^d	NPE P value ^d	NPE Q value ^e	ADRD OR ^f	ADRD P value ^f	NPE-ADRD concordant effect direction
Braak NFT stage											
2	<i>BIN1</i>	127,135,234	rs6733839	T/C	0.42	1.21	1.6×10 ⁻⁹	1.2×10 ⁻⁷	1.18	6.5×10 ⁻⁹⁰	Yes
3	<i>MME</i>	155,069,722	rs16824536	A/G	0.05	0.75	0.00016	0.0063	0.92	3.8×10 ⁻⁶	Yes
6	<i>HLA-DQA1</i>	32,615,322	rs6605556	A/G	0.16	0.85	0.00024	0.0063	0.91	1.0×10 ⁻¹⁷	Yes
CAA											
11	<i>PICALM</i>	86,157,598	rs3851179	T/C	0.35	0.89	0.00087	0.04	0.90	6.5×10 ⁻³⁶	Yes
12	<i>TPCN1</i>	113,281,983	rs6489896	T/C	0.07	1.23	0.001	0.04	1.08	2.5×10 ⁻⁶	Yes
CERAD score											
1	<i>CRI</i>	207,577,223	rs679515	T/C	0.20	1.14	0.0018	0.023	1.13	5.2×10 ⁻³³	Yes
2	<i>BIN1</i>	127,135,234	rs6733839	T/C	0.41	1.19	3.2×10 ⁻⁷	2.5×10 ⁻⁵	1.18	6.5×10 ⁻⁹⁰	Yes
2	<i>INPP5D</i>	233,117,202	rs10933431	C/G	0.22	0.88	0.0017	0.023	0.92	1.0×10 ⁻¹⁷	Yes
7	<i>ZCWPW1/NYAP1</i>	100,334,426	rs7384878	T/C	0.29	0.90	0.0032	0.031	0.93	2.1×10 ⁻¹⁸	Yes
8	<i>PTK2B</i>	27,362,470	rs73223431	T/C	0.37	1.12	0.0012	0.023	1.07	5.3×10 ⁻¹⁵	Yes
11	<i>PICALM</i>	86,157,598	rs3851179	T/C	0.35	0.84	1.1×10 ⁻⁶	4.1×10 ⁻⁵	0.90	6.5×10 ⁻³⁶	Yes
11	<i>SORL1</i>	121,564,878	rs11218343	T/C	0.04	0.78	0.0057	0.044	0.85	1.0×10 ⁻¹⁴	Yes
14	<i>FERMT2</i>	52,924,962	rs17125924	A/G	0.09	1.19	0.0038	0.033	1.09	5.8×10 ⁻¹⁰	Yes
15	<i>SNX1</i>	64,131,307	rs3848143	A/G	0.22	1.13	0.0031	0.031	1.05	1.1×10 ⁻⁶	Yes
19	<i>ABCA7</i>	1,050,875	rs12151021	A/G	0.33	1.15	0.0005	0.013	1.11	4.1×10 ⁻³⁰	Yes
Hippocampal sclerosis											
7	<i>TMEM106B</i>	12,229,967	rs13237518	A/C	0.42	0.66	6.0×10 ⁻¹¹	4.6×10 ⁻⁹	0.96	5.1×10 ⁻⁷	Yes
16	<i>IL34</i>	70,660,097	rs4985556	A/C	0.11	0.74	0.0019	0.037	1.06	5.6×10 ⁻⁶	No
17	<i>GRN</i>	44,352,876	rs5848	T/C	0.30	1.40	3.2×10 ⁻⁸	1.2×10 ⁻⁶	1.07	1.8×10 ⁻¹²	Yes
17	<i>MAPT</i>	46,779,275	rs199515	C/G	0.21	0.77	0.00034	0.0087	0.94	6.0×10 ⁻⁹	Yes
LATE-NC											
7	<i>TMEM106B</i>	12,229,967	rs13237518	A/C	0.43	0.69	6.3×10 ⁻⁸	4.8×10 ⁻⁶	0.96	5.1×10 ⁻⁷	Yes
17	<i>GRN</i>	44,352,876	rs5848	T/C	0.30	1.32	1.3×10 ⁻⁶	5.0×10 ⁻⁵	1.07	1.8×10 ⁻¹²	Yes
Microinfarct											
12	<i>TPCN1</i>	113,281,983	rs6489896	T/C	0.07	1.28	0.0013	0.049	1.08	2.5×10 ⁻⁶	Yes
16	<i>PLCG2</i>	81,739,398	rs12446759	A/G	0.39	0.87	0.00055	0.042	0.94	3.6×10 ⁻¹²	Yes

^aEither known locus or closest protein-coding gene according to GENCODE release 40. ^bEAF, effect allele frequency. ^cPosition of the lead variant using GRCh38 assembly. ^dEAF in NPE meta-analysis. ^eNPE P values and OR are from meta-analysis. ^fNPE Q values are produced by applying Benjamini-Hochberg adjustments for each endophenotype separately. ^gADRD P values and OR are from ref. 6 stage I GWAS (n=487,511). OR are with respect to the Bellenguez effect allele.

with the hypothesis that the association between [rs7247551](#) and CAA risk may be driven by hypomethylation of CpG sites in the *APOC2* region. Previous studies in other human cohorts also implicate hypomethylation at cg09555818 and cg13119609 in AD⁵⁶⁻⁵⁸. Collectively, these results provide evidence that *APOC2* may be the target gene of the [rs7247551](#) CAA risk locus, although more research must be done for verification.

We also identified associations between known loci and multiple NPEs, including *BIN1*, *APOE* and *TMEM106B*. These associations provide context regarding their involvement in disease pathogenesis. One intronic locus of *TMEM106B* was significantly associated with both hippocampal sclerosis and LATE-NC, while a locus within *GRN* was associated with hippocampal sclerosis. Both genes are associated with frontotemporal lobar degeneration with TDP-43 inclusions^{59,60}, hippocampal sclerosis^{61,62}, and were recently associated with clinical AD^{5,6}. We found that hippocampal sclerosis, LATE-NC, and clinical AD all colocalize at these two loci, suggesting that hippocampal sclerosis, LATE-NC and clinical AD likely share causal loci for these genes. Furthermore, hippocampal sclerosis (*GRN* and *TMEM106B*) and LATE-NC (*TMEM106B*) colocalized with brain eQTL and mQTL, and *TMEM106B* expression and methylation were associated with LATE-NC

in downstream analyses. Notably, lead *GRN* and *TMEM106B* variants identified in GWAS of ADRD were not associated with the ADNC NPEs. Given that a substantial fraction of individuals diagnosed with dementia have LATE-NC or hippocampal sclerosis pathology (with estimates as high as ~50%)³, it is plausible that the associations found between these genes and clinical AD in recent GWAS are due to individuals with these non-AD pathologies who were diagnosed clinically with AD.

A locus ~30 kbp downstream of *BIN1* on chr2q14 was significantly associated with Braak stage and suggestively associated with CERAD score for neuritic plaques. In previous GWAS, this locus was second only to *APOE* for strength of association with LOAD⁶. We verified through colocalization analysis that the same locus drives association signals with the Braak NFT stage and CERAD score. Interestingly, the lead variant in this locus, [rs6733839](#), was not associated with nonneuritic amyloid plaques nor CAA, neither of which include tau deposits. Previous research supports the hypothesis that *BIN1* is associated with LOAD through its effect on NFT rather than amyloid pathology^{63,64}.

We also discovered intriguing new loci mapped to *COL4A1*, *PIK3RS5* and *LZTS1* associated with atherosclerosis in the circle of Willis, Braak NFT stage and brain arteriolosclerosis, respectively.

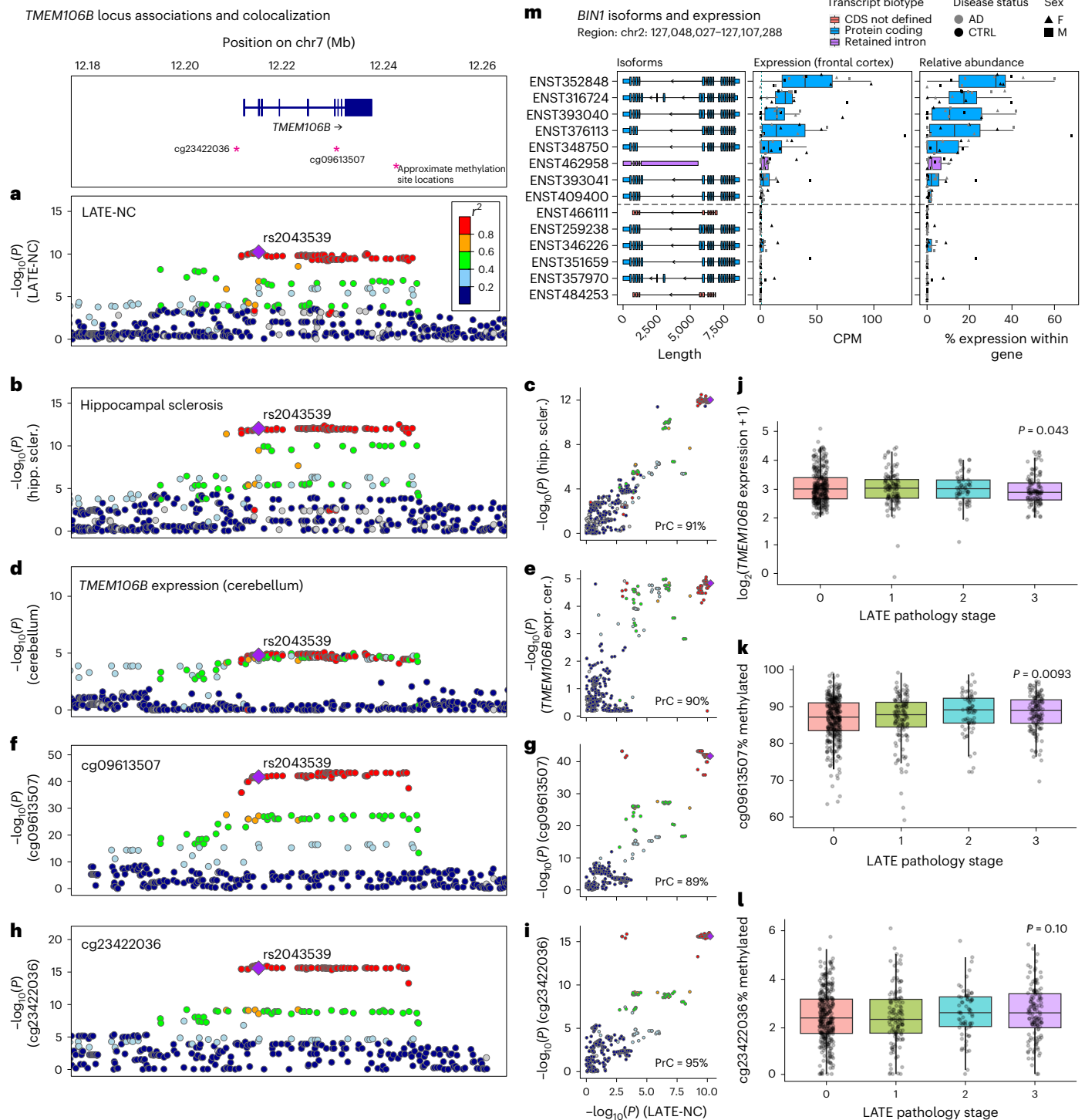


Fig. 4 | Hippocampal sclerosis and quantitative trait loci all colocalize with LATE-NC on *TMEM106B*. We investigated whether loci associated with multiple NPEs show evidence for genetic colocalization using a Bayesian colocalization analysis approach implemented in the coloc R package⁷². **a**, The *TMEM106B* lead variant (**rs2043539**) reached genome-wide significance with LATE-NC. **b,c**, Hippocampal sclerosis colocalized with LATE-NC on *TMEM106B* (PrC = 91%). **d,e**, *TMEM106B* expression colocalized with LATE-NC (PrC = 90%). **f-i**, Two methylation QTLs (mQTLs), cg09613507 (PrC = 89%; **f,g**) and cg23422036 (PrC = 95%; **h,i**), also colocalized with LATE-NC. **a, b, d, f** and **h** show regional LocusZoom⁷³ plots for each trait. Purple diamonds represent lead variants. **c, e, g** and **i** compare $-\log_{10}(P)$ values between each trait compared to LATE-NC $-\log_{10}(P)$ values across the *TMEM106B* **rs2043539** locus (color legend same as in **a**). The *TMEM106B* expression and the methylation data were obtained from

ROSMAP. **j**, Decreased *TMEM106B* expression was associated with more severe LATE-NC pathology ($P = 0.043$). Unless otherwise specified, for all boxplots, boxes outline the first quartile, median and third quartile. Whiskers extend up to 1.5× the distance between the first and third quartiles. **k**, Hypermethylation of cg09613507 was associated with more severe LATE-NC pathology ($P = 0.0093$). **l**, Methylation at cg23422036 was not significantly associated ($P = 0.10$). **m**, Unrelated to *TMEM106B*, *BIN1* expresses eight distinct RNA isoforms simultaneously in the frontal cortex from six AD cases and six controls. To understand the complexities and nuances of ADRDs, we also need to understand the nuances of the genes purported to be driving disease. CDS, coding sequence; CTRL, control; CPM, counts per million; F, female; M, male; hipp. scler., hippocampal sclerosis; expr. cer., expression in cerebellum.

APOC2 locus associations and colocalization

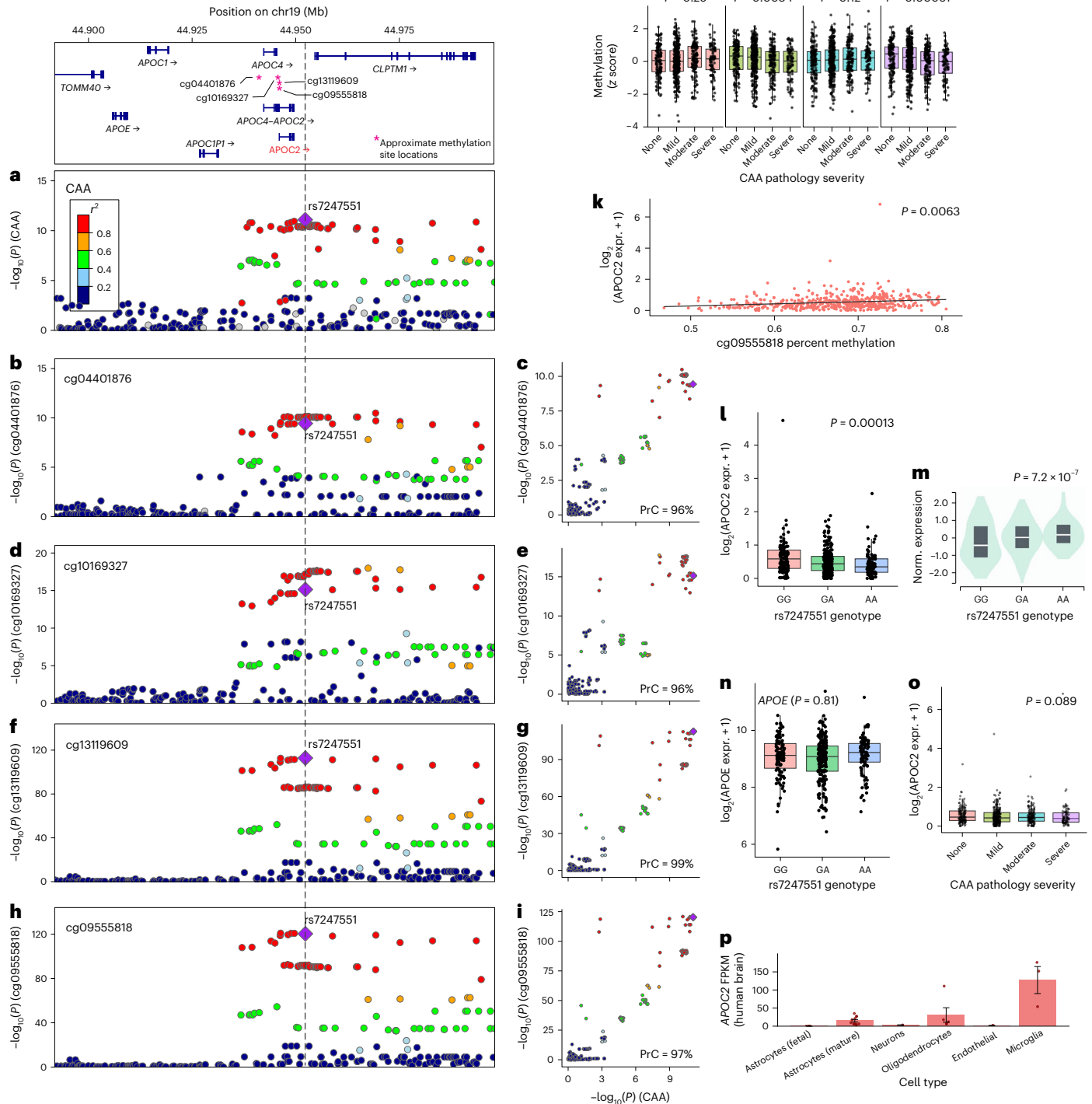


Fig. 5 | Four mQTL colocalize with CAA on *APOC2*. Using the same Bayesian colocalization analysis approach from Fig. 4 (coloc 5.2.2 R package⁷²), we tested for colocalization between CAA and methylation sites using existing data from ROSMAP. **a**, Lead SNP **rs7247551**, near *APOC2*, reached genome-wide significance with CAA. **b,d,f,h**, The **rs7247551** was also significantly associated with four mQTL. **b–i**, cg04401876 (PrC = 96%; **b,c**), cg10169327 (PrC = 96%; **d,e**), cg13119609 (PrC = 99%; **f,g**) and cg09555818 (PrC = 97%; **h,i**) all colocalized with CAA. **a, b, d, f, and h** show regional LocusZoom⁷³ plots for each trait. **c, e, g** and **i** compare $-\log_{10}(P)$ values between each trait compared to CAA $-\log_{10}(P)$ values across the *APOC2* **rs7247551** locus. Variants in LD with the lead variant (purple diamond in **a–i**) are shaded in **a–i** according to the color legend on the left-hand side of **a, j**. Plots of normalized methylation level versus CAA pathology severity. Hypomethylation at cg09555818 (OR = 0.82, $P = 0.003$) and cg13119609 (OR = 0.78, $P = 0.0006$) were significantly associated with more severe CAA

pathology. Unless otherwise specified, for all boxplots, boxes outline the first quartile, median and third quartile. Whiskers extend up to 1.5× the distance between the first and third quartiles. **k**, Both cg09555818 ($P = 0.0063$; **k**) and cg13119609 ($P = 0.0069$; not shown) were significantly associated with *APOC2* expression. **l,m**, The **rs7247551** G allele was significantly associated with increased *APOC2* expression in the frontal cortex in ROSMAP ($\beta = 0.072$, $P = 0.00013$; **l**); however, the direction of effect was opposite of that found in brain tissues in GTEx ($P = 7.2 \times 10^{-7}$; **m**). **n,o**, The **rs7247551** was not associated with *APOE* ($P = 0.81$; **n**) or *APOC2* ($P = 0.89$; **o**) expression in frontal cortex in ROSMAP. **p**, *APOC2* is highly expressed, especially in microglia and oligodendrocytes. Columns represent mean FPKM. Error bars indicate the s.e. of measurement for each cell type based on the number of human samples sequenced for each type (fetal astrocytes, $n = 6$; mature astrocytes, $n = 12$; neurons, $n = 1$; oligodendrocytes, $n = 5$; endothelial, $n = 2$ and microglia, $n = 3$). expr., expression; norm., normalized.

One locus on chr13q34 with lead variant **rs2000660** located 12 kbp upstream of *COL4A1* was significantly associated with atherosclerosis in the circle of Willis. Previous research found that the *COL4A1/COL4A2* locus is associated with numerous vascular disease phenotypes, including peripheral artery disease, coronary artery disease, stroke, arterial stiffness, rare familial cerebrovascular diseases and stroke^{65–67}. In a recent GWAS, **rs2000660** was a lead risk variant for migraines⁶⁸. The relevance of the *COL4A1* locus to cerebral vascular traits is thus highly supported by previous research, and the biological role of collagen IV in vascular disease is possibly related to the disruption of the extracellular matrix⁶⁵. *COL4A1* is preferentially expressed in astrocytes and endothelial cells and codes for a component of collagen IV, an important component of basal lamina. Endothelial cells are strongly implicated in atherosclerosis, and in recent years, researchers have suggested that astrocytes may also be directly involved in cerebrovascular disease⁶⁹. The **rs2000660** was not nominally associated with any other vascular NPE in our study, and a previous GWAS of circle of Willis atherosclerosis using ROSMAP participants did not identify the *COL4A1* as a risk locus²⁴. The **rs650724**, a variant in high LD with **rs2000660** ($r^2 = 0.84$), is a synonymous coding variant (p.Ser1600Ser in ENST00000375820.10; p.Ser319Ser in ENST00000650424.1) within *COL4A1*. The **rs2000660** is also located within an enhancer for *COL4A1*, presenting possible molecular functional mechanisms driving association in this locus.

An intronic variant within *PIK3R5* (**rs72844606**; chr17p13) was associated with the Braak NFT stage. *PIK3R5* codes for a phosphatidylinositol 3-kinase involved in cell growth, motility and survival. There is previous research suggesting that *PIK3R5* is more highly expressed in aged adults with Braak NFT stages V and VI versus nondemented controls⁷⁰. *PIK3R5* is expressed preferentially in microglial cells in humans³⁵, suggesting that its association with neurofibrillary pathology may be immune-mediated.

One new intronic locus in *LZTSL1* was found to be protective against brain arteriolosclerosis. The relatively modest literature regarding *LZTSL1* has focused mostly on cancers; however, *LZTSL1* is primarily expressed in endothelial cells and astrocytes, cell types relevant to vascular function and dysfunction. One paper suggests that *LZTSL1* is involved in neuronal delamination and development of glial-like cells during mammalian neocortical development⁷¹, but additional work related to *LZTSL1* and its function in the cerebrovasculature and brain parenchyma is needed.

In conclusion, we identified promising new loci associated with NPEs and replicated multiple known risk loci for ADRD using NPE-based GWAS. Our study demonstrates the importance of studying genetic risk factors of NPEs as a complement to studies of clinical and proxy phenotypes of LOAD.

Online content

Any methods, additional references, Nature Portfolio reporting summaries, source data, extended data, supplementary information, acknowledgements, peer review information; details of author contributions and competing interests; and statements of data and code availability are available at <https://doi.org/10.1038/s41588-024-01939-9>.

References

- Farfel, J. M. et al. Relation of genomic variants for Alzheimer disease dementia to common neuropathologies. *Neurology* **87**, 489–496 (2016).
- Katsumata, Y. et al. Multiple gene variants linked to Alzheimer's-type clinical dementia via GWAS are also associated with non-Alzheimer's neuropathologic entities. *Neurobiol. Dis.* **174**, 105880 (2022).
- Karanth, S. et al. Prevalence and clinical phenotype of quadruple misfolded proteins in older adults. *JAMA Neurol.* **77**, 1299–1307 (2020).
- Jansen, I. E. et al. Genome-wide meta-analysis identifies new loci and functional pathways influencing Alzheimer's disease risk. *Nat. Genet.* **51**, 404–413 (2019).
- Wightman, D. P. et al. A genome-wide association study with 1,126,563 individuals identifies new risk loci for Alzheimer's disease. *Nat. Genet.* **53**, 1276–1282 (2021).
- Bellenguez, C. et al. New insights into the genetic etiology of Alzheimer's disease and related dementias. *Nat. Genet.* **54**, 412–436 (2022).
- Kunkle, B. W. et al. Genetic meta-analysis of diagnosed Alzheimer's disease identifies new risk loci and implicates A β , tau, immunity and lipid processing. *Nat. Genet.* **51**, 414–430 (2019).
- Escott-Price, V. & Hardy, J. Genome-wide association studies for Alzheimer's disease: bigger is not always better. *Brain Commun.* **4**, fcac125 (2022).
- Karran, E. & De Strooper, B. The amyloid hypothesis in Alzheimer disease: new insights from new therapeutics. *Nat. Rev. Drug Discov.* **21**, 306–318 (2022).
- Nelson, P. T., Braak, H. & Markesbery, W. R. Neuropathology and cognitive impairment in Alzheimer disease: a complex but coherent relationship. *J. Neuropathol. Exp. Neurol.* **68**, 1–14 (2009).
- Yang, H. S. et al. Evaluation of TDP-43 proteinopathy and hippocampal sclerosis in relation to APOE ϵ 4 haplotype status: a community-based cohort study. *Lancet Neurol.* **17**, 773–781 (2018).
- Nelson, P. T. et al. Limbic-predominant age-related TDP-43 encephalopathy (LATE): consensus working group report. *Brain* **142**, 1503–1527 (2019).
- Nelson, P. T. et al. Frequency of LATE neuropathologic change across the spectrum of Alzheimer's disease neuropathology: combined data from 13 community-based or population-based autopsy cohorts. *Acta Neuropathol.* **144**, 27–44 (2022).
- Brenowitz, W. D. et al. Hippocampal sclerosis of aging is a key Alzheimer's disease mimic: clinical-pathologic correlations and comparisons with both Alzheimer's disease and non-tauopathic frontotemporal lobar degeneration. *J. Alzheimers Dis.* **39**, 691–702 (2014).
- Skrobot, O. A. et al. Vascular cognitive impairment neuropathology guidelines (VCING): the contribution of cerebrovascular pathology to cognitive impairment. *Brain* **139**, 2957–2969 (2016).
- Weber, S. A., Patel, R. K. & Lutsep, H. L. Cerebral amyloid angiopathy: diagnosis and potential therapies. *Expert Rev. Neurother.* **18**, 503–513 (2018).
- Smith, E. E. et al. Cerebral microinfarcts: the invisible lesions. *Lancet Neurol.* **11**, 272–282 (2012).
- Arvanitakis, Z. et al. The relationship of cerebral vessel pathology to brain microinfarcts. *Brain Pathol.* **27**, 77–85 (2017).
- Neltner, J. H. et al. Arteriolosclerosis that affects multiple brain regions is linked to hippocampal sclerosis of ageing. *Brain* **137**, 255–267 (2014).
- Arvanitakis, Z. et al. Relation of cerebral vessel disease to Alzheimer's disease dementia and cognitive function in elderly people: a cross-sectional study. *Lancet Neurol.* **15**, 934–943 (2016).
- Ighodaro, E. T. et al. Risk factors and global cognitive status related to brain arteriolosclerosis in elderly individuals. *J. Cereb. Blood Flow Metab.* **37**, 201–216 (2017).
- Beecham, G. W. et al. Genome-wide association meta-analysis of neuropathologic features of Alzheimer's disease and related dementias. *PLoS Genet.* **10**, e1004606 (2014).
- Shade, L. M. et al. Genome-wide association study of brain arteriolosclerosis. *J. Cereb. Blood Flow Metab.* **42**, 1437–1450 (2022).
- Vattathil, S. M. et al. A genetic study of cerebral atherosclerosis reveals novel associations with NTNG1 and CNOT3. *Genes (Basel)* **12**, 815 (2021).

25. Farrell, K. et al. Genome-wide association study and functional validation implicates JADE1 in tauopathy. *Acta Neuropathol.* **143**, 33–53 (2022).
26. Reddy, J. S. et al. Genome-wide analysis identifies a novel LINC-PINT splice variant associated with vascular amyloid pathology in Alzheimer's disease. *Acta Neuropathol. Commun.* **9**, 93 (2021).
27. Nelson, P. T. et al. ABCC9 gene polymorphism is associated with hippocampal sclerosis of aging pathology. *Acta Neuropathol.* **127**, 825–843 (2014).
28. Rüb, U. et al. The evolution of Alzheimer's disease-related cytoskeletal pathology in the human raphe nuclei. *Neuropathol. Appl. Neurobiol.* **26**, 553–567 (2000).
29. Mirra, S. S. et al. The Consortium to Establish a Registry for Alzheimer's Disease (CERAD). Part II. Standardization of the neuropathologic assessment of Alzheimer's disease. *Neurology* **41**, 479–486 (1991).
30. Besser, L. M. et al. The revised National Alzheimer's Coordinating Center's neuropathology form—available data and new analyses. *J. Neuropathol. Exp. Neurol.* **77**, 717–726 (2018).
31. Attems, J. et al. Neuropathological consensus criteria for the evaluation of Lewy pathology in post-mortem brains: a multi-centre study. *Acta Neuropathol.* **141**, 159–172 (2021).
32. Montine, T. J. et al. National Institute on Aging–Alzheimer's Association guidelines for the neuropathologic assessment of Alzheimer's disease: a practical approach. *Acta Neuropathol.* **123**, 1–11 (2012).
33. Willer, C. J., Li, Y. & Abecasis, G. R. METAL: fast and efficient meta-analysis of genomewide association scans. *Bioinformatics* **26**, 2190–2191 (2010).
34. Shinohara, M. et al. Impact of sex and APOE4 on cerebral amyloid angiopathy in Alzheimer's disease. *Acta Neuropathol.* **132**, 225–234 (2016).
35. Zhang, Y. et al. Purification and characterization of progenitor and mature human astrocytes reveals transcriptional and functional differences with mouse. *Neuron* **89**, 37–53 (2016).
36. Zhang, Y. et al. An RNA-sequencing transcriptome and splicing database of glia, neurons, and vascular cells of the cerebral cortex. *J. Neurosci.* **34**, 11929–11947 (2014).
37. Watanabe, K. et al. Functional mapping and annotation of genetic associations with FUMA. *Nat. Commun.* **8**, 1826 (2017).
38. Pollard, K. S. et al. Detection of nonneutral substitution rates on mammalian phylogenies. *Genome Res.* **20**, 110–121 (2010).
39. Giambartolomei, C. et al. Bayesian test for colocalisation between pairs of genetic association studies using summary statistics. *PLoS Genet.* **10**, e1004383 (2014).
40. Katsumata, Y. et al. LATE-NC risk alleles (in TMEM106B, GRN, and ABCC9 genes) among persons with African ancestry. *J. Neuropathol. Exp. Neurol.* **82**, 760–768 (2023).
41. Dugan, A. J. et al. Analysis of genes (TMEM106B, GRN, ABCC9, KCNMB2, and APOE) implicated in risk for LATE-NC and hippocampal sclerosis provides pathogenetic insights: a retrospective genetic association study. *Acta Neuropathol. Commun.* **9**, 152 (2021).
42. Ng, B. et al. An xQTL map integrates the genetic architecture of the human brain's transcriptome and epigenome. *Nat. Neurosci.* **20**, 1418–1426 (2017).
43. Kelemen, O. et al. Function of alternative splicing. *Gene* **514**, 1–30 (2013).
44. Keren, H., Lev-Maor, G. & Ast, G. Alternative splicing and evolution: diversification, exon definition and function. *Nat. Rev. Genet.* **11**, 345–355 (2010).
45. Kim, E., Magen, A. & Ast, G. Different levels of alternative splicing among eukaryotes. *Nucleic Acids Res.* **35**, 125–131 (2007).
46. Aguzzoli-Heberle, B. et al. Mapping medically relevant RNA isoform diversity in the aged human frontal cortex with deep long-read RNA-seq. *Nat. Biotechnol.* <https://doi.org/10.1038/s41587-024-02245-9> (2024).
47. Ciolli Mattioli, C. et al. Alternative 3' UTRs direct localization of functionally diverse protein isoforms in neuronal compartments. *Nucleic Acids Res.* **47**, 2560–2573 (2019).
48. Weber, R. et al. Monitoring the 5'UTR landscape reveals isoform switches to drive translational efficiencies in cancer. *Oncogene* **42**, 638–650 (2023).
49. Zhang, Q. & Tian, B. The emerging theme of 3'UTR mRNA isoform regulation in reprogramming of cell metabolism. *Biochem. Soc. Trans.* **51**, 1111–1119 (2023).
50. Dickson, D. W. et al. APOE ϵ 4 is associated with severity of Lewy body pathology independent of Alzheimer pathology. *Neurology* **91**, e1182–e1195 (2018).
51. Shih, Y. H. et al. TDP-43 interacts with amyloid- β , inhibits fibrillization, and worsens pathology in a model of Alzheimer's disease. *Nat. Commun.* **11**, 5950 (2020).
52. Wolska, A. et al. Apolipoprotein C-II: new findings related to genetics, biochemistry, and role in triglyceride metabolism. *Atherosclerosis* **267**, 49–60 (2017).
53. Jong, M. C., Hofker, M. H. & Havekes, L. M. Role of ApoCs in lipoprotein metabolism: functional differences between ApoC1, ApoC2, and ApoC3. *Arterioscler. Thromb. Vasc. Biol.* **19**, 472–484 (1999).
54. Ben Braiek, A. et al. Identification of biomarker panels as predictors of severity in coronary artery disease. *J. Cell. Mol. Med.* **25**, 1518–1530 (2021).
55. Cervantes, S. et al. Genetic variation in APOE cluster region and Alzheimer's disease risk. *Neurobiol. Aging* **32**, 2107.e7–2107.e17 (2011).
56. Walker, R. M. et al. Identification of epigenome-wide DNA methylation differences between carriers of APOE ϵ 4 and APOE ϵ 2 alleles. *Genome Med.* **13**, 1 (2021).
57. Walker, R. M. et al. Epigenome-wide analyses identify DNA methylation signatures of dementia risk. *Alzheimers Dement. (Amst.)* **12**, e12078 (2020).
58. Shao, Y. et al. DNA methylation of TOMM40–APOE–APOC2 in Alzheimer's disease. *J. Hum. Genet.* **63**, 459–471 (2018).
59. Rollinson, S. et al. Frontotemporal lobar degeneration genome wide association study replication confirms a risk locus shared with amyotrophic lateral sclerosis. *Neurobiol. Aging* **32**, 758.e1–758.e7 (2011).
60. Ciani, M. et al. Genome wide association study and next generation sequencing: a glimmer of light toward new possible horizons in frontotemporal dementia research. *Front. Neurosci.* **13**, 506 (2019).
61. Katsumata, Y. et al. Gene-based association study of genes linked to hippocampal sclerosis of aging neuropathology: GRN, TMEM106B, ABCC9, and KCNMB2. *Neurobiol. Aging* **53**, 193.e17–193.e25 (2017).
62. Nelson, P. T. et al. Reassessment of risk genotypes (GRN, TMEM106B, and ABCC9 variants) associated with hippocampal sclerosis of aging pathology. *J. Neuropathol. Exp. Neurol.* **74**, 75–84 (2015).
63. Holler, C. J. et al. Bridging integrator 1 (BIN1) protein expression increases in the Alzheimer's disease brain and correlates with neurofibrillary tangle pathology. *J. Alzheimers Dis.* **42**, 1221–1227 (2014).
64. Franzmeier, N. et al. The BIN1 rs744373 SNP is associated with increased tau-PET levels and impaired memory. *Nat. Commun.* **10**, 1766 (2019).
65. Steffensen, L. B. & Rasmussen, L. M. A role for collagen type IV in cardiovascular disease? *Am. J. Physiol. Heart Circ. Physiol.* **315**, H610–H625 (2018).

66. Blevins, B. L. et al. Brain arteriolosclerosis. *Acta Neuropathol.* **141**, 1–24 (2021).
67. Rannikmäe, K. et al. COL4A2 is associated with lacunar ischemic stroke and deep ICH: meta-analyses among 21,500 cases and 40,600 controls. *Neurology* **89**, 1829–1839 (2017).
68. Hautakangas, H. et al. Genome-wide analysis of 102,084 migraine cases identifies 123 risk loci and subtype-specific risk alleles. *Nat. Genet.* **54**, 152–160 (2022).
69. Price, B. R. et al. An emerging role of astrocytes in vascular contributions to cognitive impairment and dementia. *J. Neurochem.* **144**, 644–650 (2018).
70. Guennewig, B. et al. Defining early changes in Alzheimer's disease from RNA sequencing of brain regions differentially affected by pathology. *Sci. Rep.* **11**, 4865 (2021).
71. Kawaue, T. et al. Lzts1 controls both neuronal delamination and outer radial glial-like cell generation during mammalian cerebral development. *Nat. Commun.* **10**, 2780 (2019).
72. Wang, G. et al. A simple new approach to variable selection in regression, with application to genetic fine mapping. *J. R. Stat. Soc. Ser. B Stat. Methodol.* **82**, 1273–1300 (2020).
73. Pruim, R. J. et al. LocusZoom: regional visualization of genome-wide association scan results. *Bioinformatics* **26**, 2336–2337 (2010).

Publisher's note Springer Nature remains neutral with regard to jurisdictional claims in published maps and institutional affiliations.

Open Access This article is licensed under a Creative Commons Attribution-NonCommercial-NoDerivatives 4.0 International License, which permits any non-commercial use, sharing, distribution and reproduction in any medium or format, as long as you give appropriate credit to the original author(s) and the source, provide a link to the Creative Commons licence, and indicate if you modified the licensed material. You do not have permission under this licence to share adapted material derived from this article or parts of it. The images or other third party material in this article are included in the article's Creative Commons licence, unless indicated otherwise in a credit line to the material. If material is not included in the article's Creative Commons licence and your intended use is not permitted by statutory regulation or exceeds the permitted use, you will need to obtain permission directly from the copyright holder. To view a copy of this licence, visit <http://creativecommons.org/licenses/by-nc-nd/4.0/>.

© The Author(s) 2024

¹Department of Biostatistics, College of Public Health, University of Kentucky, Lexington, KY, USA. ²Sanders-Brown Center on Aging and Alzheimer's Disease Research Center, University of Kentucky, Lexington, KY, USA. ³Department of Epidemiology and Environmental Health, College of Public Health, University of Kentucky, Lexington, KY, USA. ⁴Department of Neuroscience, University of Kentucky College of Medicine, Lexington, KY, USA. ⁵Vanderbilt Memory and Alzheimer's Center, Department of Neurology, Vanderbilt University Medical Center, Nashville, TN, USA. ⁶Vanderbilt Genetics Institute, Vanderbilt University Medical Center, Nashville, TN, USA. ⁷Department of Medicine, University of Washington, Seattle, WA, USA. ⁸Department of Neurology, Columbia University, New York City, NY, USA. ⁹Department of Medicine (Biomedical Genetics), Boston University Chobanian and Avedisian School of Medicine, Boston, MA, USA. ¹⁰Department of Neurology, Boston University Chobanian and Avedisian School of Medicine, Boston, MA, USA. ¹¹Department of Ophthalmology, Boston University Chobanian and Avedisian School of Medicine, Boston, MA, USA. ¹²Department of Biostatistics, School of Public Health, Boston University, Boston, MA, USA. ¹³Department of Epidemiology, School of Public Health, Boston University, Boston, MA, USA. ¹⁴Department of Pathology and Laboratory Medicine, University of Pennsylvania Perelman School of Medicine, Philadelphia, PA, USA. ¹⁵Penn Neurodegeneration Genomics Center, University of Pennsylvania Perelman School of Medicine, Philadelphia, PA, USA. ¹⁶Cleveland Institute for Computational Biology, Case Western Reserve University, Cleveland, OH, USA. ¹⁷Department of Population and Quantitative Health Sciences, Case Western Reserve University, Cleveland, OH, USA. ¹⁸National Alzheimer's Coordinating Center, Department of Epidemiology, University of Washington, Seattle, WA, USA. ¹⁹Department of Radiology and Imaging Sciences, Indiana University School of Medicine, Indianapolis, IN, USA. ²⁰Indiana Alzheimer's Disease Research Center, Indiana University School of Medicine, Indianapolis, IN, USA. ²¹Center for Computational Biology and Bioinformatics, Indiana University School of Medicine, Indianapolis, IN, USA. ²²Center for Neuroimaging, Department of Radiology and Imaging Sciences, Indiana University School of Medicine, Indianapolis, IN, USA. ²³Department of Neurological Sciences, Rush Medical College, Chicago, IL, USA. ²⁴Rush Alzheimer's Disease Center, Rush Medical College, Chicago, IL, USA. ²⁵Department of Pathology, Rush Medical College, Chicago, IL, USA. ²⁶Division of Biomedical Informatics, Department of Internal Medicine, University of Kentucky College of Medicine, Lexington, KY, USA. ²⁷Department of Pathology and Laboratory Medicine, University of Kentucky College of Medicine, Lexington, KY, USA. ²⁸These authors jointly supervised this work: Mark T. W. Ebbert, Peter T. Nelson, David W. Fardo. ✉e-mail: david.fardo@uky.edu

The National Alzheimer's Coordinating Center

Walter A. Kukull¹⁷, Andrew J. Saykin^{19,21} & David A. Bennett²²

The Alzheimer's Disease Genetics Consortium

David W. Fardo^{1,2,28}, Erin L. Abner^{2,3}, Subhabrata Mukherjee⁶, Richard P. Mayeux⁷, Lindsay A. Farrer^{8,9,10,11,12}, Gerard D. Schellenberg^{13,14}, Jonathan L. Haines^{15,16}, Walter A. Kukull¹⁷, David A. Bennett^{22,23} & Julie A. Schneider^{22,23,24}

A full list of members appears in the Supplementary Information.

Methods

Participants

An overview of our study design is presented in Fig. 1. Each participating study previously obtained informed consent from participants or caregivers for participants with substantial cognitive impairment. Parent study protocols were approved by the local institutional review boards. This study was approved by the University of Kentucky Office of Research Integrity Institutional Review Board.

NACC. The present study used NACC data from 36 National Institute on Aging (NIA)-funded Alzheimer's Disease Research Centers (ADRCs). Individual ADRCs use different recruitment strategies and perform autopsies on-site, but neuropathology data at each ADRC are collected using a standard form (<https://files.alz.washington.edu/documentation/np11-form.pdf>) and submitted to NACC where they are aggregated and anonymized. The NACC Neuropathology dataset based on the first version of this form was originally implemented in 2001 (ref. 30), and this analysis uses data from then through the March 2023 freeze. Participants were excluded if they did not have autopsy data available or if they were noted in the NACC Neuropathology dataset to have at least one of 19 conditions that could potentially bias results. These conditions include brain tumors, severe head trauma and frontotemporal lobar degeneration (see Supplementary Table 6 for the full list of variables used for exclusion criteria).

ROSMAP. ROSMAP consists of harmonized data from the following two longitudinal cohort studies: the Religious Orders Study (ROS) and the Rush Memory and Aging Project (MAP)⁷⁴. ROS and MAP were both approved by the Institutional Review Board of Rush University Medical Center. All participants signed the Uniform Anatomic Gift Act, as well as informed and repository consents. ROS began in 1994 and has recruited over 1,500 Catholic priests, nuns and brothers across the United States. MAP started in 1997 and has enrolled more than 2,300 community members in the greater Chicago area of northeastern Illinois. The ROSMAP NP data used in this study were received from Rush University Medical Center in January 2020. Using KING 2.2.7 (ref. 75), we found that several participants in ROSMAP also had neuropathology and genotype data available in NACC. In these cases, records in the NACC were preferentially kept.

ACT. The ACT study began in 1994 and recruited residents in the greater Seattle area aged 65 years and older without dementia at the time of enrollment^{76–79}. The study has expanded to include three cohorts with continued enrollment using the original enrollment criteria and has a current total of 4,960 participants across all three cohorts. The ACT NP data used in this study were obtained from Kaiser Permanente in May 2023.

Genotype data and quality control

Genotype data for all cohorts underwent imputation using the Trans-Omics for Precision Medicine (TOPMed) Imputation Server 1.7.3 and the TOPMed reference panel using Minimac 4 (refs. 80–82). Postprocessing was performed with BCFtools 1.10.2 (ref. 83) and SAMtools 1.10 (ref. 84), PLINK 1.9 and 2.0 (ref. 85), R 4.2.1 and 4.2.2 (<https://cran.r-project.org/>), and R packages `data.table` 1.14.10 (<https://CRAN.R-project.org/package=data.table>) and `stringi` 1.803 (ref. 86). The 3.4.2 NACC and ACT raw genotype data were obtained from the September 2020 freeze of the Alzheimer's Disease Genetics Consortium (ADGC) in March 2021 and subsequently imputed. Pre-imputed ROSMAP genotype data were received from collaborators in the Hohman Lab at Vanderbilt University in December 2021. Genetic variants with minor allele frequency (MAF) < 0.1% and imputation quality scores of < 0.8 were removed before further quality control measures. Due to the small sample sizes of participants with substantial non-European ancestry (based on proximity to 1000 Genomes 'EUR' superpopulation

cluster in principal component (PC) analysis), especially in replication cohorts, these participants were excluded from the analysis. Standard GWAS quality control procedures were followed for variant and participant inclusion (Supplementary Methods).

Defining and harmonizing NPEs for analysis

In total, we combined and/or harmonized 11 NPEs for analysis across the four studies. We note that there are differences in the way that some neuropathological data were collected across studies, and our strategy for harmonizing was informed by practical considerations for maximizing available sample sizes given the available endophenotypes. Thus, several synthetic NPEs were created by merging existing NPEs within a cohort or by harmonizing categorical variables from one cohort and continuous variables from another. Hippocampal sclerosis, microinfarcts and gross infarcts were recorded as binary case-control phenotypes. Arteriosclerosis, atherosclerosis, CAA, CERAD score for neuritic plaques, amyloid plaques, LATE-NC and Lewy body pathology were recorded as four-stage ordinal variables that either measured progressive severity of pathology ('none' < 'mild' < 'moderate' < 'severe') or progressing anatomical distribution of pathology. Braak NFT was recorded as a seven-stage ordinal variable that followed the anatomical distributional stages originally characterized in ref. 87. We provide a deeper description of our harmonization approach in the Supplementary Methods, and a detailed listing of variables harmonized across data sources to construct NPEs for analysis is available in Supplementary Table 1.

To assess the co-occurrence of NPEs in our data, we estimated polychoric correlations (an approach that assumes that observed ordinal or binary variables reflect latent normally distributed variables) between NPE pairs, followed by hierarchical clustering using the `polycor` 0.8-1 (ref. 88), `psych`⁸⁹ and `pheatmap` 1.0.12 (ref. 90) R packages (Extended Data Fig. 1).

DNA methylation data

Preprocessed and quality-controlled DNA methylation data for 740 ROSMAP participants were downloaded from Synapse.org (Synapse IDs: syn3157275 and syn3191087). DNA methylation preparation and quality control measures have been previously described^{91,92}. Briefly, approximately 50 mg of frozen gray matter tissue from the DLPFC was sampled from each participant. DNA was then extracted and processed using the Illumina Infinium HumanMethylation450 BeadChip. Quality control measures included removing low-quality probes, removing participants with poor bisulfite-conversion efficiency and adjusting methylation levels by age, sex and batch, which adequately controlled for batch effects⁹². Missing methylation levels were imputed using 100-nearest neighbors^{91,92}.

RNA-seq data

Preprocessed and quality-controlled bulk-tissue RNA-seq data from the DLPFC of ROSMAP participants were downloaded from Synapse.org (Synapse IDs: syn21088596, syn21323366, syn3505732 and syn3505724). As previously described, samples were prepared by sectioning approximately 100 mg of gray matter tissue from the DLPFC and RNA extracted using the Qiagen MiRNeasy Mini (217004) protocol and then submitted for transcriptome library construction using the dUTP protocol and Illumina sequencing⁹². A total of 634 participants in seven batches were sequenced with an average sequencing depth of 50 million paired reads per sample⁹². Subsequent quality control and batch corrections were performed, and the final output of the RNA-Seq pipeline was fragments per kilobase of transcript per million mapped reads (FPKM)⁹².

Statistical analyses

Single-variant GWAS. We analyzed ordinal endophenotypes using proportional-odds logistic mixed-effects models implemented in the

POLMM 0.2.3 (refs. 93,94) and GRAB 0.1.1 R packages⁹³ and analyzed binary variables similarly with logistic mixed-effects models implemented in the SAIGE R package⁹⁵. Fixed-effect covariates included age at death, sex, cohort and the first ten genetic PCs created using the PCA in Related Samples (PC-AiR) method in the GENESIS 2.26.0 R package⁹⁶. We included a dense genetic relationship matrix (GRM) as a random effect to account for relatedness between participants. An additive mode of inheritance was assumed in all analyses.

Analysis of individual data sources proceeded in two stages. In stage one, GRM was constructed using a pruned set of independent variants, defined as having a pairwise $r^2 < 0.2$ within moving windows of 15 kbp. Null models, which included fixed covariates and the GRM, were then fitted using the GWASTools 1.42.1 (ref. 97), SNPRelate 1.30.1 (ref. 98), POLMM 0.2.3 (refs. 93,94), GRAB 0.1.1 (refs. 93,94) and/or SAIGE 1.1.3 (ref. 95) R packages. In stage two, score tests were performed on each variant with a saddle-point approximation used to calculate P values. We considered all variants with a $P < 5 \times 10^{-8}$ to be genome-wide significant. To identify independent risk loci, we clumped results using the ‘-clump’ flag in PLINK 1.9 with the pairwise LD threshold set to $r^2 \leq 0.05$ (<https://www.cog-genomics.org/plink/1.9>)⁸⁵. Following analyses of individual cohorts, we performed fixed-effects meta-analyses using METAL software using inverse-variance weighting on variants with MAF > 1% in each cohort³³.

Conditional analysis of the APOE region. The region surrounding the *APOE* gene on chr19 is consistently the single strongest genetic risk factor for LOAD in GWAS. Three common forms of the *APOE* gene— $\epsilon 2$, $\epsilon 3$ and $\epsilon 4$ —are present in our study populations (see Table 1 for distribution of *APOE* alleles in participants), and the $\epsilon 2$ and $\epsilon 4$ alleles are associated with lower and higher risk of LOAD, respectively, relative to the $\epsilon 3$ allele⁹⁹. We therefore expected that variants in the *APOE* region, defined as the region within 200 kbp from the start and end transcription sites of *APOE*, would be associated with multiple NPEs in our study. Moreover, we hypothesized that genetic variants in the *APOE* region may influence neuropathology risk independently of the effects of *APOE* ϵ alleles. To test this hypothesis, we re-analyzed variants in chr19 while adjusting for *APOE* ϵ diplotype. We limited re-analysis to endophenotypes with at least one genome-wide significant association signal within the *APOE* locus in the final meta-analysis of the three independent GWAS. *APOE* diplotypes were determined either using the rs7412 and rs429358 variants according to the SNPedia online ref. 100 or taken directly from study data if available. Both rs7412 and rs429358 variants had high imputation quality scores ($r^2 = 0.997$ and 0.975 , respectively). The $\epsilon 3/\epsilon 3$ diplotype was used as a reference, and we included fixed-effect indicator variables to adjust for $\epsilon 2/\epsilon 2$, $\epsilon 2/\epsilon 3$, $\epsilon 3/\epsilon 4$ and $\epsilon 4/\epsilon 4$ diplotypes. We chose this approach rather than adjusting for counts of $\epsilon 2$ and $\epsilon 4$ alleles because it is robust to potential nonlinear effects of genotypes. We performed additional sensitivity analyses for loci identified through this approach (Supplementary Information).

Replication of known AD risk loci in NPE. We used the 83 ADRD loci presented in a recent large GWAS to investigate whether AD-associated loci were associated with NPE⁶. We restricted our comparison to AD loci with lead variants with MAF ≥ 0.01 , which excluded three loci, leaving 76 loci for comparison. LD for variants near the top-known AD-associated variants was evaluated using the R package LDLinkR 1.2.3 (ref. 101). We controlled the false-discovery rate for each NPE using the Benjamini–Hochberg procedure¹⁰². Variants with an adjusted Q value ≤ 0.05 were considered significant.

FUMA and FAVOR annotation, gene-prioritization and functional enrichment pipeline. We mapped variants to genes and performed subsequent gene and gene-set analyses using the FUMA and FAVOR pipelines^{37,103}. Variants were mapped to genes if they had $P \leq 1 \times 10^{-5}$

in the GWAS meta-analysis and were located within 10 kbp of a protein-coding gene’s transcription start or end sites. Gene-based analyses were performed using MAGMA 1.10. The top variant PCs that accounted for 99.9% of the variance in a gene’s region were used to test for significance using an F test. We considered genes with resulting $P \leq 2.5 \times 10^{-6}$ to be significantly associated with NPE. Gene-set enrichment analyses were performed using MAGMA¹⁰⁴ gene-set analysis of Gene Ontology and curated gene sets from MSigDB¹⁰⁵. Bonferroni P value corrections were made for each NPE individually.

Colocalization analyses. We used multiple sources of publicly available summary statistics from external studies as data sources for Bayesian colocalization analyses. First, we downloaded Genotype-Tissue Expression Project (GTEx) v8 European ancestry QTL analysis summary statistics, which contains summary statistics for significant gene expression and splicing QTL variants (eQTL and sQTL, respectively) in 48 body tissues¹⁰⁶. We also used gene expression and DNA mQTL analysis summary statistics from studies using tissue from the DLPFC of ROSMAP participants⁴². These studies examined the associations of genetic variants with molecular traits and provided curated lists of significant QTL variants. Finally, we downloaded the summary statistics from a recent GWAS of LOAD for a targeted *post hoc* colocalization analysis in *TMEM106B* and *GRN*⁶.

For each NPE outcome in our study, we first created a list of genetic variants with $P \leq 1 \times 10^{-5}$ in the GWAS meta-analysis. We then queried the lists of significant QTL variants in GTEx and ROSMAP using R (<https://cran.r-project.org/>) and Python 3.8.16 and 3.10.8 (<https://www.python.org/>) to identify neuropathology-associated QTL variants. For each genetic locus associated with NPEs that had at least one significant QTL in either GTEx or ROSMAP, we performed colocalization analysis using the ‘coloc.abf’ function in the coloc 5.2.2R package³⁹. For ordinal variables, we chose dichotomizing cut points to determine case–control proportions. We used coloc’s default prior PrC of PrC = 1×10^{-5} and considered a posterior PrC > 80% as a threshold for evidence of colocalization.

To investigate whether shared GWAS signals drive association among multiple NPEs, we also performed colocalization analysis on loci with variants satisfying $P < 1 \times 10^{-4}$ and concordant effect direction for at least two NPEs in the GWAS meta-analysis. Due to the absence of associations in the region in *APOE*-adjusted analyses for NPEs other than CAA, we excluded that region for NPE–NPE colocalization analyses.

Association analyses using DLPFC DNA methylation and bulk RNA-seq data from ROSMAP. ROSMAP participants had postmortem bulk-tissue samples collected from the DLPFC, which underwent DNA methylation quantification using the Illumina DNAMethylation450 chip and gene expression and RNA-seq using the Illumina HiSeq 2000 (ref. 92). In total, 708 ROSMAP participants had DNA methylation data available for analysis. We restricted analyses involving DNA methylation or RNA-seq data to NPE-associated loci that reached the genome-wide significance threshold in the meta-analysis and also colocalized with mQTL or eQTL in brain tissue in either GTEx or ROSMAP.

In our *APOE* ϵ -adjusted genetic association analysis, one locus near *APOE* remained significantly associated with CAA. This locus colocalized with DNA methylation levels at four CpG sites in ROSMAP. To investigate whether these CpG sites were in turn associated with CAA pathology, we combined individual-level DNA methylation and neuropathological data in ROSMAP for analysis. We used cumulative logit models using the ‘clm’ function implemented in the R package ordinal 2023.13.12-04 (ref. 107) with the semi-quantitative CAA variable described above as the outcome for analysis. We performed four analyses, with one of each of the four CpG sites tested as the independent variable of interest in each analysis. We adjusted for age, sex, ROS versus MAP study, bisulfite-conversion efficiency, postmortem interval and *APOE* ϵ diplotype in each analysis. Similar models were used to test associations between hippocampal sclerosis and LATE-NC and methylation levels at

CpG sites cg09613507 and cg23422036. Wald tests were performed on the resulting parameter estimates to test for statistical significance. We also performed post hoc analyses examining the association between these CpG sites and *APOC2* expression in ROSMAP.

For genes with significant eQTL in GTEx or ROSMAP that colocalized with NPE, we performed additional targeted analyses to assess the association between gene expression and NPE. We first assessed the association between NPE lead variants and gene expression in ROSMAP to confirm nominal eQTL status. We then performed generalized linear regression models between square-root or log-transformed mRNA expression and NPE outcomes adjusting for age at death, sex, PMI and RNA integrity number.

Plots from these analyses were generated using the R package *ggplot2* (ref. 108).

Replication of CAA locus using Mayo Clinic neuropathology GWAS. We used data from Mayo Clinic Brain Bank participants available from ref. 26 study of the genetic risk factors of CAA (dataset heretofore referred to as MC-CAA) to attempt to replicate a new CAA locus in the present study in an independent sample²⁶. Neuropathology and genetic variant data were downloaded from Synapse (Synapse IDs: syn10930250, syn21499318, syn21522653 and syn21547862). Eight participants were identified as duplicates between batches or with NACC participants and removed. While CAA is graded on a four-level ordinal scale in the present study, CAA in MC-CAA is graded as an average of CAA burden across five brain regions²⁶. We therefore used linear regression with the outcome variable as $\sqrt{\text{CAA}}$ with the independent variable of interest being the number of G alleles of variant [rs7247551](#). Covariates included *APOE* diplotypes ($\epsilon 3/\epsilon 3$, $\epsilon 2/\epsilon 4$, $\epsilon 2/\epsilon 3$, $\epsilon 3/\epsilon 4$ or $\epsilon 4/\epsilon 4$), sex, age at death (truncated at 90 years) and the first three genetic PCs.

Reporting summary

Further information on research design is available in the Nature Portfolio Reporting Summary linked to this article.

Data availability

Meta-analysis summary statistics for each NPE studied will be made available through NIAGADS upon publication at <https://dss.niagads.org/>. The authors are unable to share genotype or phenotype data from NACC, ADGC, ROSMAP or ACT due to data use restrictions. While these data were de-identified for study authors, these studies contain identifiable information on participants. ROSMAP data can be requested at <https://www.radc.rush.edu> and <https://www.synapse.org>. ADGC data can be requested from NIAGADS at <https://www.niagads.org/resources/related-projects/alzheimers-disease-genetics-consortium-adgc-collection>. NACC neuropathology data can be requested at <https://naccdata.org/>. ACT data can be requested at <https://actagingresearch.org/>. Harmonized neuropathology data are available through NIAGADS at <https://dss.niagads.org/datasets/ng00067/>. The results published here are in whole or in part based on data obtained from the AD Knowledge Portal. Raw long-read RNA-seq data generated and used in this manuscript are publicly available in both Synapse (<https://www.synapse.org/#!Synapse:syn52047893>) and NIH SRA (accession: [SRP456327](#)). Processed long-read RNA-seq data can be easily downloaded or viewed at https://ebbertlab.com/brain_rna_isoform_seq.html.

Code availability

All code used for data preparation and analysis is available at <https://doi.org/10.5281/zenodo.11089995> (ref. 109).

References

74. Bennett, D. A. et al. Religious Orders Study and Rush Memory and Aging Project. *J. Alzheimers Dis.* **64**, S161–s189 (2018).

75. Manichaikul, A. et al. Robust relationship inference in genome-wide association studies. *Bioinformatics* **26**, 2867–2873 (2010).
76. Kukull, W. A. et al. Dementia and Alzheimer disease incidence: a prospective cohort study. *Arch. Neurol.* **59**, 1737–1746 (2002).
77. Postupna, N. et al. The delayed neuropathological consequences of traumatic brain injury in a community-based sample. *Front. Neurol.* **12**, 624696 (2021).
78. Sonnen, J. A. et al. Neuropathology in the adult changes in thought study: a review. *J. Alzheimers Dis.* **18**, 703–711 (2009).
79. Crane, P. K. et al. Alzheimer's disease sequencing project discovery and replication criteria for cases and controls: data from a community-based prospective cohort study with autopsy follow-up. *Alzheimers Dement.* **13**, 1410–1413 (2017).
80. Taliun, D. et al. Sequencing of 53,831 diverse genomes from the NHLBI TOPMed program. *Nature* **590**, 290–299 (2021).
81. Howie, B. et al. Fast and accurate genotype imputation in genome-wide association studies through pre-phasing. *Nat. Genet.* **44**, 955–959 (2012).
82. Das, S. et al. Next-generation genotype imputation service and methods. *Nat. Genet.* **48**, 1284–1287 (2016).
83. Li, H. A statistical framework for SNP calling, mutation discovery, association mapping and population genetical parameter estimation from sequencing data. *Bioinformatics* **27**, 2987–2993 (2011).
84. Danecek, P. et al. Twelve years of SAMtools and BCFtools. *GigaScience* **10**, giab008 (2021).
85. Chang, C. C. et al. Second-generation PLINK: rising to the challenge of larger and richer datasets. *GigaScience* **4**, 7 (2015).
86. Gagolewski, M. stringi: fast and portable character string processing in R. *J. Stat. Softw.* **103**, 1–59 (2022).
87. Braak, H. & Braak, E. Neuropathological staging of Alzheimer-related changes. *Acta Neuropathol.* **82**, 239–259 (1991).
88. Fox, J. polycor: polychoric and polyserial correlations. R package version 0.8-1 <https://r-forge.r-project.org/projects/polycor> (2022).
89. Revelle, W. psych: procedures for psychological, psychometric, and personality research. R package version 2.3.3 <https://CRAN.R-project.org/package=psych> (2023).
90. Kolde, R. et al. raivokolde/pheatmap. *GitHub* <https://github.com/raivokolde/pheatmap> (2018).
91. Yu, L. et al. Association of brain DNA methylation in SORL1, ABCA7, HLA-DRB5, SLC24A4, and BIN1 with pathological diagnosis of Alzheimer disease. *JAMA Neurol.* **72**, 15–24 (2015).
92. De Jager, P. L. et al. A multi-omic atlas of the human frontal cortex for aging and Alzheimer's disease research. *Sci. Data* **5**, 180142 (2018).
93. Bi, W. et al. Efficient mixed model approach for large-scale genome-wide association studies of ordinal categorical phenotypes. *Am. J. Hum. Genet.* **108**, 825–839 (2021).
94. Bi, W. et al. Scalable mixed model methods for set-based association studies on large-scale categorical data analysis and its application to exome-sequencing data in UK Biobank. *Am. J. Hum. Genet.* **110**, 762–773 (2023).
95. Zhou, W. et al. Efficiently controlling for case-control imbalance and sample relatedness in large-scale genetic association studies. *Nat. Genet.* **50**, 1335–1341 (2018).
96. Conomos, M. P., Miller, M. B. & Thornton, T. A. Robust inference of population structure for ancestry prediction and correction of stratification in the presence of relatedness. *Genet. Epidemiol.* **39**, 276–293 (2015).
97. Gogarten, S. M. et al. GWASTools: an R/Bioconductor package for quality control and analysis of genome-wide association studies. *Bioinformatics* **28**, 3329–3331 (2012).
98. Zheng, X. et al. A high-performance computing toolset for relatedness and principal component analysis of SNP data. *Bioinformatics* **28**, 3326–3328 (2012).

99. Reiman, E. M. et al. Exceptionally low likelihood of Alzheimer's dementia in APOE2 homozygotes from a 5,000-person neuropathological study. *Nat. Commun.* **11**, 667 (2020).
100. Cariaso, M. & Lennon, G. SNPedia: a wiki supporting personal genome annotation, interpretation and analysis. *Nucleic Acids Res.* **40**, D1308–D1312 (2012).
101. Myers, T. A., Chanock, S. J. & Machiela, M. J. LDlinkR: an R package for rapidly calculating linkage disequilibrium statistics in diverse populations. *Front. Genet.* **11**, 157 (2020).
102. Benjamini, Y. & Hochberg, Y. Controlling the false discovery rate: a practical and powerful approach to multiple testing. *J. R. Stat. Soc. Ser. B Stat. Methodol.* **57**, 289–300 (1995).
103. Zhou, H. et al. FAVOR: functional annotation of variants online resource and annotator for variation across the human genome. *Nucleic Acids Res.* **51**, D1300–D1311 (2023).
104. De Leeuw, C. A. et al. MAGMA: generalized gene-set analysis of GWAS data. *PLoS Comput. Biol.* **11**, e1004219 (2015).
105. Liberzon, A. et al. Molecular signatures database (MSigDB) 3.0. *Bioinformatics* **27**, 1739–1740 (2011).
106. Battle, A. et al. Genetic effects on gene expression across human tissues. *Nature* **550**, 204–213 (2017).
107. Christensen, R. H. B. Ordinal: regression models for ordinal data. R package version 2023.12-04 <https://CRAN.R-project.org/package=ordinal> (2023).
108. Wickham, H. *ggplot2: Elegant Graphics for Data Analysis* (Springer-Verlag, 2016).
109. Shade, L. M. Code for Genome-wide association study of multiple neuropathology endophenotypes identifies novel risk loci and provides insights into genetic risk of dementia. *Zenodo* <https://doi.org/10.5281/zenodo.11089995> (2024).

Acknowledgements

We disclosed receipt of the following financial support for the research, authorship and/or publication of this article: RF1AG082339 (to Y.K., S.A.C., M.T.W.E., P.T.N. and D.W.F.), R56AG057191 (to Y.K., S.A.C. and D.W.F.), F30NS124136 (to L.M.P.S.), P30 AG028383 (to P.T.N.), R35GM138636 (to B.A.H., J.A.B., M.L.P. and M.T.W.E.), R01AG068331 (to B.A.H., J.A.B., M.L.P. and M.T.W.E.), U01AG058654 (to J.L.H.), P01AG078116 (to Y.K. and K.Z.A.), K25AG055620 (to S.M.), R01AG082730 (to S.M. and D.W.F.), R01LM012535 (to K.N.), U19AG024904 (to A.J.S.), U01AG068057 (to A.J.S.), U01AG072177 (to A.J.S.), U19AG074879 (to K.N. and A.J.S.), U24AG072122 (to W.A.K.), P30AG072976 (to A.J.S.), the BrightFocus Foundation (A2020161S to M.T.W.E.), Alzheimer's Association (2019-AARG-644082 to M.T.W.E.), the University of Kentucky Center for Clinical and Translational Science TL-1 Fellowship (TL1TR0019970), the National Center for Advancing Translational Sciences (UL1TR001998) and the Dean of the College of Medicine, University of Kentucky. The content is solely the responsibility of the authors and does not necessarily represent the official views of the National Institutes of Health (NIH), the University of Kentucky or other participating institutions. The NACC database is funded by NIA/NIH under grant U01AG016976. NACC data are contributed by the NIA-funded ADCs—P30 AG019610 (E. Reiman), P30 AG013846 (N. Kowall), P50 AGO08702 (S. Small), P50 AGO25688 (A. Levey), P50 AGO47266 (T. Golde), P30 AG010133 (A. Saykin), P50 AGO05146 (M. Albert), P50 AGO05134 (B. Hyman), P50 AGO16574 (R. Petersen), P50 AGO05138 (M. Sano), P30 AGO08051 (T. Wisniewski), P30 AGO13854 (R. Vassar), P30 AGO08017 (J. Kaye), P30 AGO10161 (D. Bennett), P50 AGO47366 (V. Henderson), P30 AGO10129 (C. DeCarli), P50 AGO16573 (F. LaFerla), P50 AGO05131 (J. Brewer), P50 AGO23501 (B. Miller), P30 AGO35982 (R. Swerdlow), P30 AGO28383 (P.L. Van Eldik), P30 AGO53760 (H. Paulson), P30 AGO10124 (J. Trojanowski), P50 AGO05133 (O. Lopez), P50 AGO05142 (H. Chui), P30 AGO12300 (R. Rosenberg), P30 AGO49638 (S. Craft), P50 AGO05136 (T. Grabowski), P50 AGO33514 (S. Asthana), P50

AGO05681 (J. Morris) and P50 AGO47270 (S. Strittmatter). The results published here are in part based on data obtained from the AD Knowledge Portal. Genotyping was supported by the ADGC through the National Institute of Aging (U01AG032984 and RC2AG036528). See Supplementary Note for full ADGC acknowledgments. Samples from the National Cell Repository for Alzheimer's Disease, which receives government support under a cooperative agreement grant (U24AG21886) awarded by the NIA, were used in this study. We thank contributors who collected samples used in this study, as well as patients and their families whose help and participation made this work possible. Data for this study were prepared, archived and distributed by the National Institute on Aging Alzheimer's Disease Data Storage Site (NIAGADS) at the University of Pennsylvania (U24AG041689-01). We thank the study participants and staff of the Rush Alzheimer's Disease Center. The ROS and the Rush MAP are supported by grants from the NIH (P30AG10161, P30AG72975, R01AG15819, R01AG17917, R01AG22018, R01AG33678, R01AG34374, R01AG36042, R01AG40039, R01AG042210, U01AG46152, U01AG61356, R01AG47976, R01AG43379, R01AG54057, R01AG56352, R01NS78009 and UH2NS100599) and the Illinois Department of Public Health. The ACT study was funded by the NIA (U19AG066567). Data collection for this work was additionally supported, in part, by previous funding from the NIA (U01AG006781). All statements in this report, including its findings and conclusions, are solely those of the authors and do not necessarily represent the views of the NIA or the NIH. We thank the participants of the ACT study for the data they have provided and the many ACT investigators and staff who steward that data. You can learn more about ACT at <https://actagingstudy.org/>.

Author contributions

L.M.P.S. conceptualized study design, prepared data, performed analyses and contributed to manuscript preparation. Y.K. and S.M. provided feedback on analyses and contributed to the manuscript. Y.K. also provided software for data preparation. K.Z.A. assisted with creating figures. Q.Q. assisted with gene-based and gene-prioritization analyses and assisted with creating figures. S.A.C. and M.T.W.E. helped with data interpretation and preparing figures, and contributed to manuscript preparation. E.L.A. provided guidance on the interpretation of *BIN1* results and provided extensive feedback on manuscript preparation. B.A.H., J.A.B. and M.L.P. performed RNA isoform sequencing and analyses. T.J.H. performed imputation and quality control on ROSMAP genotype data. K.N. and A.J.S. provided imputed and quality-controlled ADNI genotype data used in an earlier version of the manuscript and provided feedback on manuscript preparation. D.A.B. and J.A.S. provided ROSMAP neuropathology data and made critical revisions to the manuscript. P.T.N. provided guidance on defining NPEs and contributed to the manuscript. D.W.F. conceptualized the study design and contributed to manuscript preparation. P.T.N., M.T.W.E. and D.W.F. jointly supervised the study. NACC and ADGC consortia provided data for their respective studies. All authors read and approved the final manuscript.

Competing interests

J.A.S. reported personal fees from the Observational Study Monitoring Board Framingham, Observational Study Monitoring Board Discovery (National Institute of Neurological Disorders and Stroke) and Takeda Pharma. A.J.S. reported support from Avid Radiopharmaceuticals, a subsidiary of Eli Lilly (in kind contribution of positron emission tomography tracer precursor), and participated in Scientific Advisory Boards (Bayer Oncology, Eisai, Novo Nordisk and Siemens Medical Solutions) and an Observational Study Monitoring Board (MESA, NIH NHLBI), as well as several other NIA External Advisory Committees. He also serves as editor-in-chief of Brain Imaging and Behavior, a Springer Nature Journal. He was not involved in the editorial handling of this Nature Genetics paper (journals within the Springer Nature Portfolio

are editorially independent). The other authors declare no competing interests.

Additional information

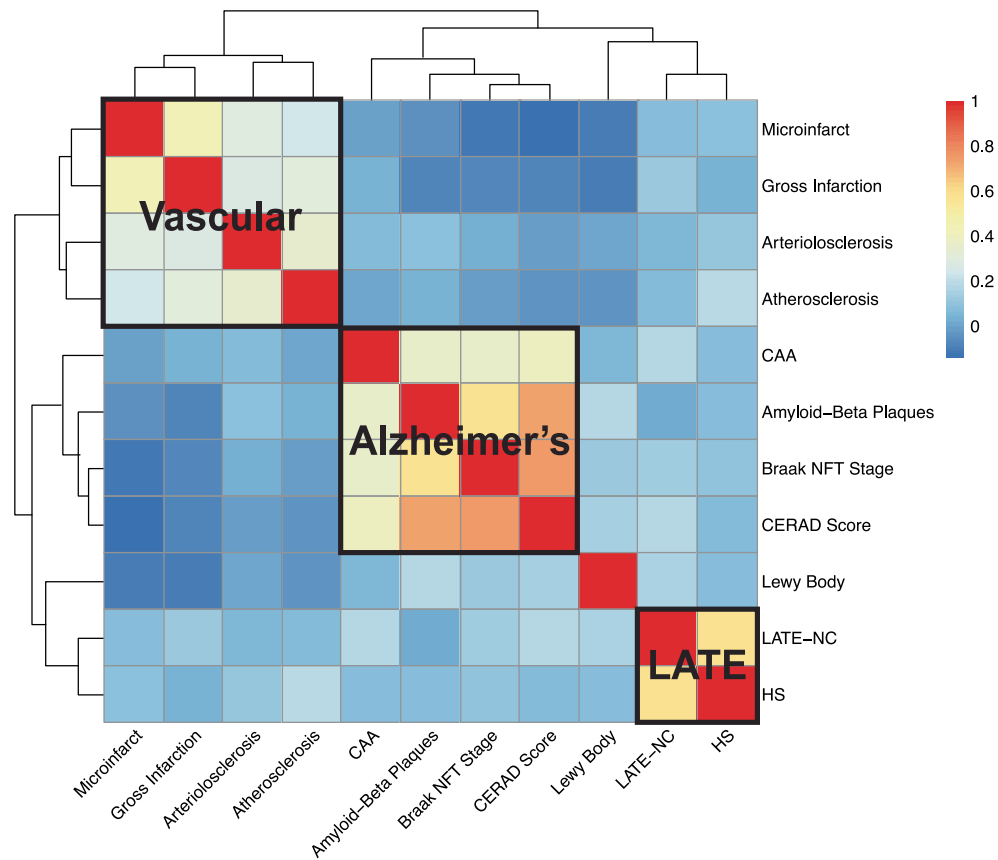
Extended data is available for this paper at <https://doi.org/10.1038/s41588-024-01939-9>.

Supplementary information The online version contains supplementary material available at <https://doi.org/10.1038/s41588-024-01939-9>.

Correspondence and requests for materials should be addressed to David W. Fardo.

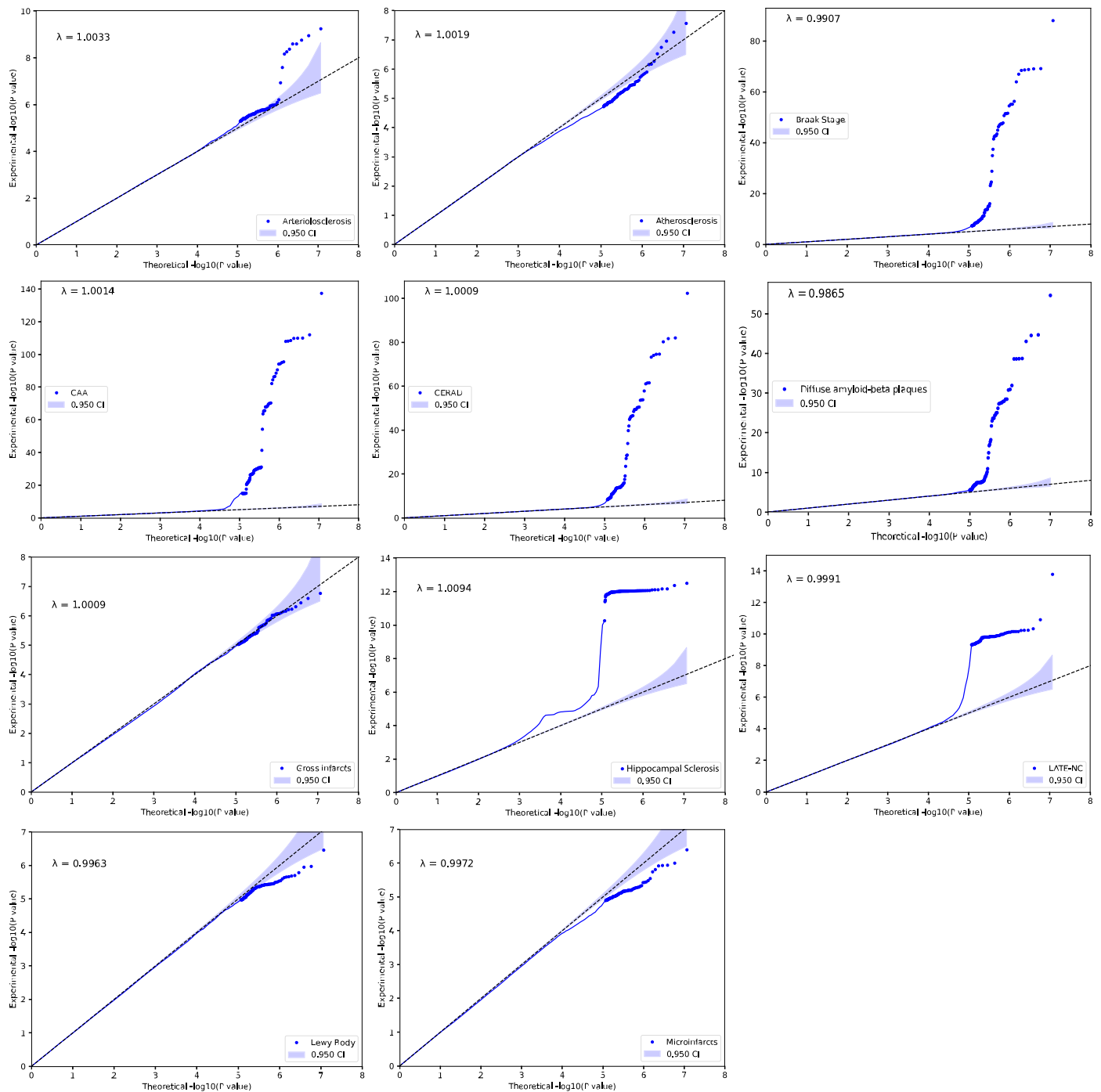
Peer review information *Nature Genetics* thanks Lasse Pihlstrom and the other, anonymous, reviewer(s) for their contribution to the peer review of this work.

Reprints and permissions information is available at www.nature.com/reprints.



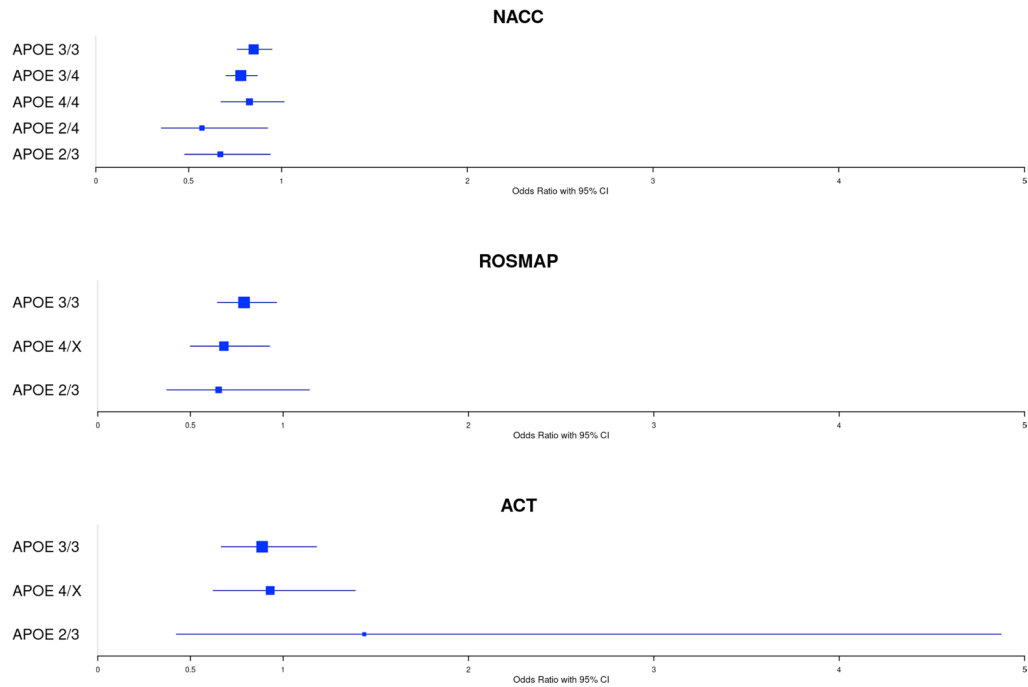
Extended Data Fig. 1 | Heatmap of the polychoric correlations of 11 neuropathology endophenotypes. The y-axis (rows) and x-axis (columns) refer to the neuropathology endophenotype pairs with the hierarchical clustering generated by the polychoric correlations calculation. The red and blue color refers to high and low correlations between the neuropathology endophenotype pairs. The three positively correlated clusters of endophenotypes that match

general expectations are highlighted by the black solid lines: a 'vascular' cluster consisting of gross infarcts, microinfarcts, arteriolosclerosis and atherosclerosis; an 'Alzheimer's disease' cluster consisting of Braak NFT stage, neuritic plaques, amyloid-beta plaques and CAA; and a 'LATE' cluster consisting of LATE-NC and HS, respectively.



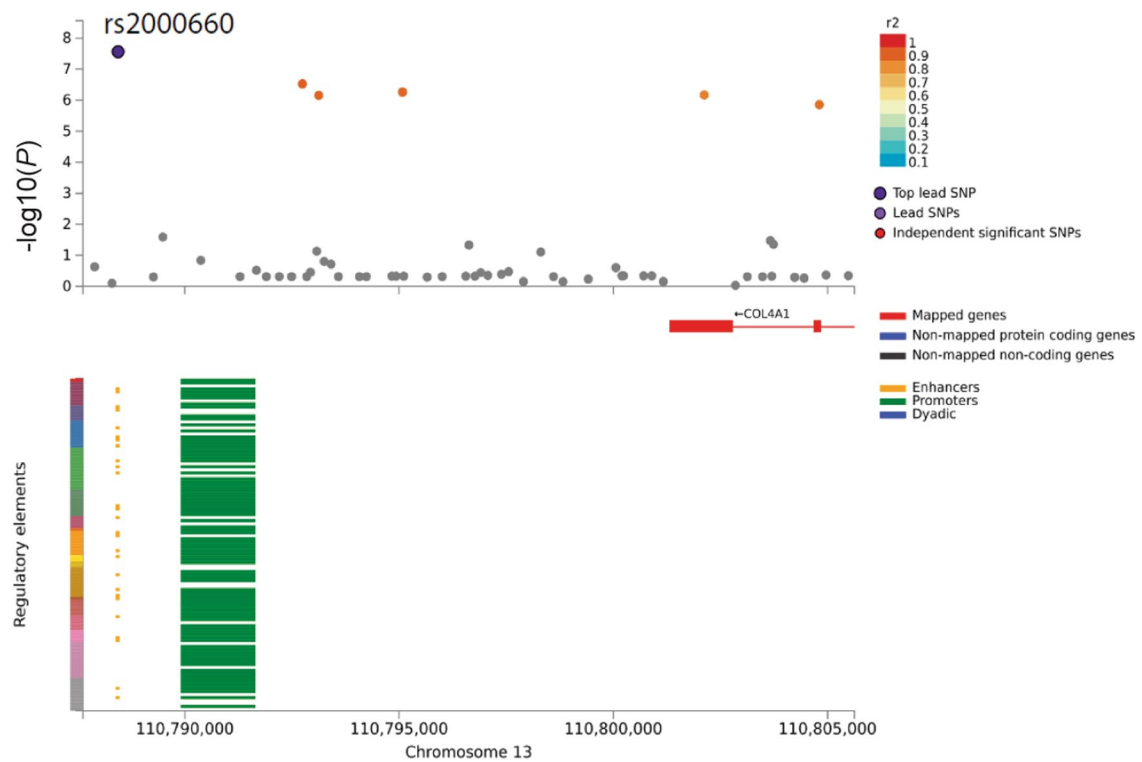
Extended Data Fig. 2 | Quantile-quantile (QQ) plots for the 11 neuropathology endophenotype. The y-axis refers to the experimental $-\log_{10}(P)$ from two-sided z test of the genome-wide association study (GWAS) meta-analysis. The x-axis refers to the theoretical $-\log_{10}(P)$ based on percentile. Each point represents a single-nucleotide polymorphism (SNP). The line of identity ($y = x$) is shown in a black dashed line, indicating the expected alignment

under the null hypothesis. Deviations from this line suggest possible inflation due to population structure or polygenic effects. The genomic inflation factor lambda (λ) is calculated for each phenotype indicating minimal inflation of test statistics. The λ estimates ranged from 0.9907 to 1.0094, and visual inspection of the QQ plots did not suggest any systematic bias in the data.



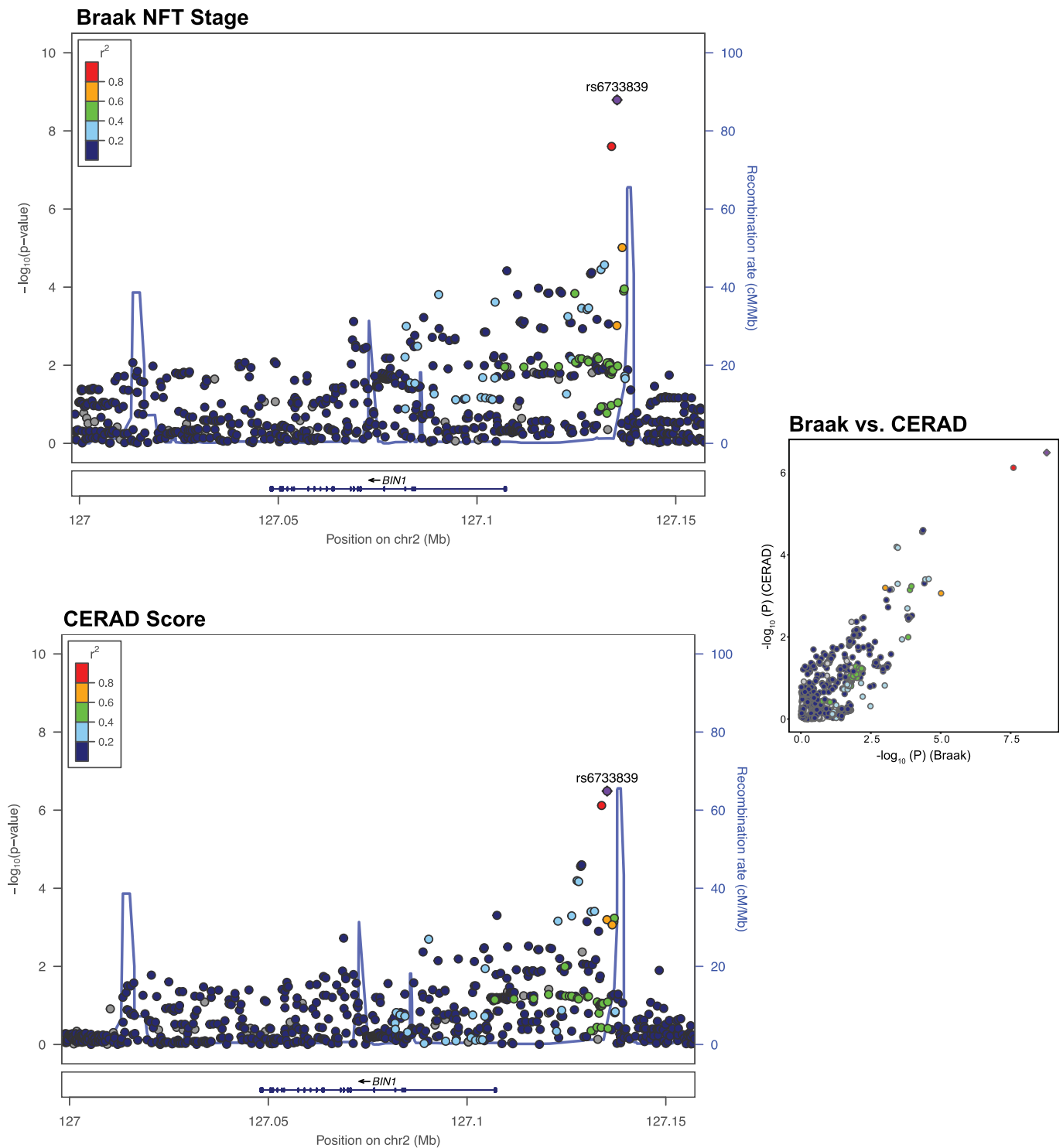
Extended Data Fig. 3 | Forest plots of associations between CAA and lead variant ([rs7247551](#)) on chromosome 19 stratified by study and *APOE* ε diplotype. For each of the data sources (NACC $n = 5,927$, ROSMAP $n = 1,172$ and ACT $n = 677$), we re-analyzed the association between CAA and lead variant [rs7247551](#) from the meta-analysis while stratifying by *APOE* ε diplotype and visually compared effect sizes across groups. Due to low sample sizes preventing

model convergence, *APOE* ε4 carriers (diplotypes ε2/ε4, ε3/ε4, ε4/ε4) were merged in analyses for ROSMAP and ACT. Points along the x-axis represent the estimated odds ratios, and error bars indicate 95% CI. Results demonstrate a consistent pattern of association between [rs7247551](#) and CAA within each of the data sources used in our study.



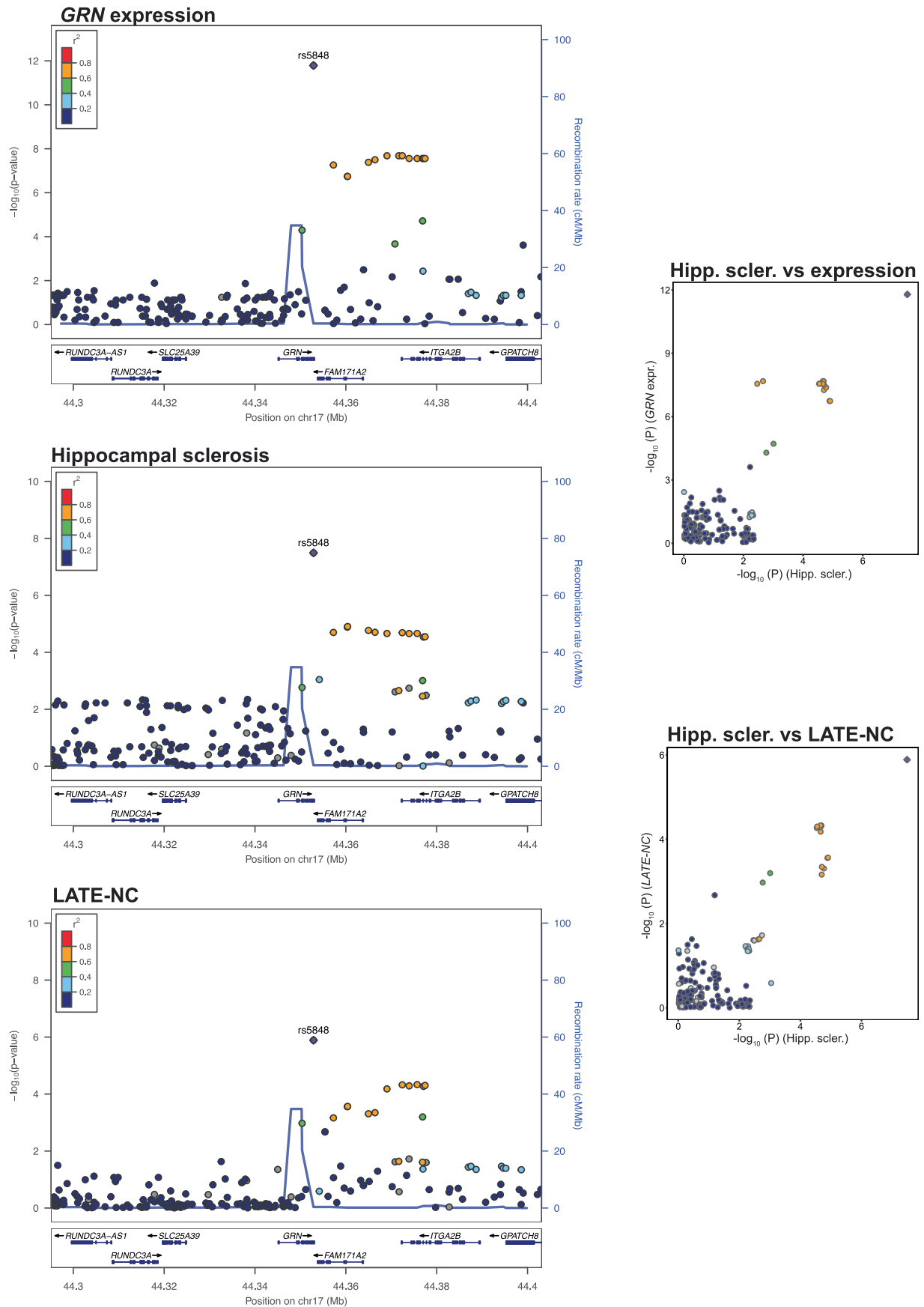
Extended Data Fig. 4 | Regional plot and the chromatin interaction plot of rs2000660 that is associated with cerebral atherosclerosis. Atherosclerosis association plot from NPE GWAS meta-analysis ($n = 7,340$) for the SNP of rs2000660. The x-axis refers to the position of the genome. In the top plot, the y-axis refers to the $-\log_{10}(P)$ from meta-analysis two-sided Z test. The lead variant, rs2000660, is circled in black and colored in dark purple. Variants meeting the

threshold of $P < 1 \times 10^{-5}$ were colored according to linkage disequilibrium r^2 to rs200060. Other variants are colored in gray. The figures are generated by FUMA pipelines (<https://fuma.ctglab.nl>). In the bottom plot, the x-axis refers to the genome position, and the y-axis refers to the type of regulatory elements in the chromatin interaction plot for rs2000660.



Extended Data Fig. 5 | CERAD score and Braak NFT stage colocalize on *BIN1*. Braak stage and CERAD association plot from NPE GWAS meta-analysis ($n = 7,776$) for the region around *BIN1*. Colored dots represent the chromosomal position (x-axis, Mb, megabase) in hg38 coordinates and $-\log_{10}(P)$ from meta-analysis two-sided z test; y-axis) of each variant in the region. Dots are colored to represent the linkage disequilibrium r^2 with the lead variant (purple dot) estimated with

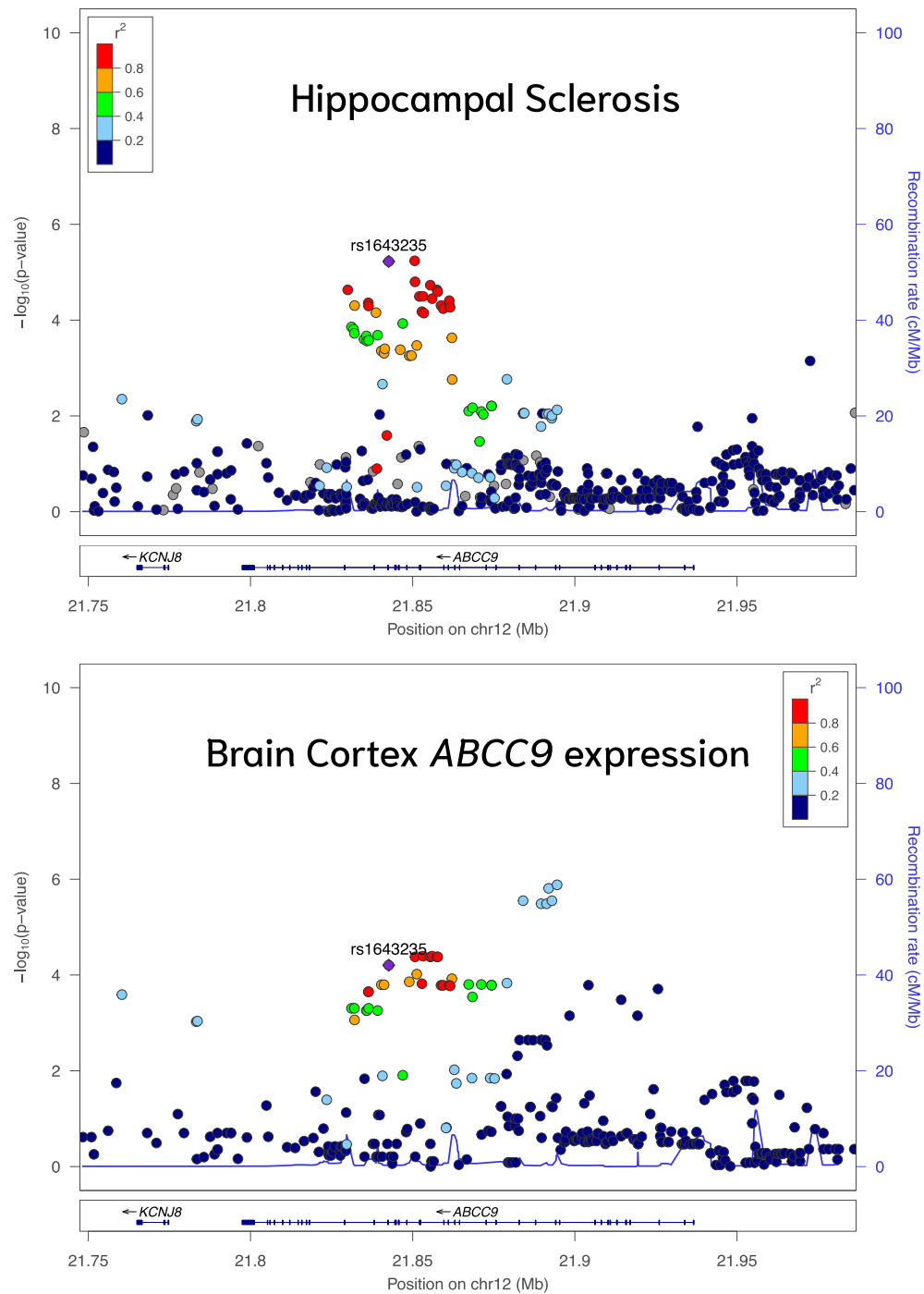
PLINK- r^2 using 1000 Genomes Phase 3 European-descended participants. The recombination rate was calculated using GRCh38 genetic map files downloaded from https://bochet.gcc.biostat.washington.edu/beagle/genetic_maps/. Boxes below data indicate the location of genes in the region (plot generated using LocusZoom⁷³).



Extended Data Fig. 6 | See next page for caption.

Extended Data Fig. 6 | *GRN* expression, hippocampal sclerosis and LATE-NC all colocalize on *GRN*. *GRN* gene expression, hippocampal sclerosis and LATE-NC association plot from NPE GWAS meta-analysis ($n = 7,776$) for the region around *GRN*. Colored dots represent the chromosomal position (x-axis, Mb, megabase) in hg38 coordinates and $-\log_{10}(P)$ from meta-analysis two-sided z test; y-axis) of each variant in the region. Dots are colored to represent the

linkage disequilibrium r^2 with the lead variant (purple dot) estimated with PLINK-r2 using 1000 Genomes Phase 3 European-descended participants. The recombination rate was calculated using GRCh38 genetic map files downloaded from https://bochet.gcc.biostat.washington.edu/beagle/genetic_maps/. Boxes below data indicate the location of genes in the region (plot generated using LocusZoom⁷³).



Extended Data Fig. 7 | Hippocampal sclerosis and *ABCC9* expression colocalize on *ABCC9*. *ABCC9* gene expression and hippocampal sclerosis association plot from NPE GWAS meta-analysis ($n = 7,776$) for the region around *ABCC9*. Colored dots represent the chromosomal position (x-axis, Mb, megabase) in hg38 coordinates and $-\log_{10}(P$ from meta-analysis two-sided Z test; y-axis) of each variant in the region. Dots are colored to represent the

linkage disequilibrium r^2 with the lead variant (purple dot) estimated with PLINK-r2 using 1000 Genomes Phase 3 European-descended participants. The recombination rate was calculated using GRCh38 genetic map files downloaded from https://bochet.gcc.biostat.washington.edu/beagle/genetic_maps/. Boxes below data indicate the location of genes in the region (plot generated using LocusZoom⁷³).

Reporting Summary

Nature Portfolio wishes to improve the reproducibility of the work that we publish. This form provides structure for consistency and transparency in reporting. For further information on Nature Portfolio policies, see our [Editorial Policies](#) and the [Editorial Policy Checklist](#).

Statistics

For all statistical analyses, confirm that the following items are present in the figure legend, table legend, main text, or Methods section.

- | n/a | Confirmed |
|-------------------------------------|--|
| <input type="checkbox"/> | <input checked="" type="checkbox"/> The exact sample size (n) for each experimental group/condition, given as a discrete number and unit of measurement |
| <input type="checkbox"/> | <input checked="" type="checkbox"/> A statement on whether measurements were taken from distinct samples or whether the same sample was measured repeatedly |
| <input type="checkbox"/> | <input checked="" type="checkbox"/> The statistical test(s) used AND whether they are one- or two-sided
<i>Only common tests should be described solely by name; describe more complex techniques in the Methods section.</i> |
| <input type="checkbox"/> | <input checked="" type="checkbox"/> A description of all covariates tested |
| <input type="checkbox"/> | <input checked="" type="checkbox"/> A description of any assumptions or corrections, such as tests of normality and adjustment for multiple comparisons |
| <input type="checkbox"/> | <input checked="" type="checkbox"/> A full description of the statistical parameters including central tendency (e.g. means) or other basic estimates (e.g. regression coefficient) AND variation (e.g. standard deviation) or associated estimates of uncertainty (e.g. confidence intervals) |
| <input type="checkbox"/> | <input checked="" type="checkbox"/> For null hypothesis testing, the test statistic (e.g. F , t , r) with confidence intervals, effect sizes, degrees of freedom and P value noted
<i>Give P values as exact values whenever suitable.</i> |
| <input type="checkbox"/> | <input checked="" type="checkbox"/> For Bayesian analysis, information on the choice of priors and Markov chain Monte Carlo settings |
| <input checked="" type="checkbox"/> | <input type="checkbox"/> For hierarchical and complex designs, identification of the appropriate level for tests and full reporting of outcomes |
| <input type="checkbox"/> | <input checked="" type="checkbox"/> Estimates of effect sizes (e.g. Cohen's d , Pearson's r), indicating how they were calculated |

Our web collection on [statistics for biologists](#) contains articles on many of the points above.

Software and code

Policy information about [availability of computer code](#)

Data collection	No software was used .
Data analysis	bcftools 1.10.2 KING 2.2.7 MAGMA 1.10 METAL 2011-03-25 Minimac 4 PLINK 1.9 and 2.0 Python 3.8.16 and 3.10.8 R 4.2.1 and 4.2.2 R package coloc 5.2.2 R package data.table 1.14.10 R package GENESIS 2.26.0 R package ggplot2 3.4.2 R package GRAB 0.1.1 R package GWASTools 1.42.1 R package LDlinkR 1.2.3 R package MASS 7.3-60 R package mediation 4.5.0 R package ordinal 2023.12-04 R package pheatmap 1.012

R package psych 2.3.3
 R package POLMM 0.2.3
 R package SAIGE 1.1.3
 R package SNPRelate 1.30.1
 R package stringi 1.8.3
 samtools 1.10
 TOPMed Imputation Server 1.7.3

For manuscripts utilizing custom algorithms or software that are central to the research but not yet described in published literature, software must be made available to editors and reviewers. We strongly encourage code deposition in a community repository (e.g. GitHub). See the Nature Portfolio [guidelines for submitting code & software](#) for further information.

Data

Policy information about [availability of data](#)

All manuscripts must include a [data availability statement](#). This statement should provide the following information, where applicable:

- Accession codes, unique identifiers, or web links for publicly available datasets
- A description of any restrictions on data availability
- For clinical datasets or third party data, please ensure that the statement adheres to our [policy](#)

Code used for data preparation and analysis is available at <https://zenodo.org/doi/10.5281/zenodo.11089995>.

Meta-analysis summary statistics for each neuropathology endophenotype studied will be made available through NIAGADS upon publication at <https://www.niagads.org/>.

ROSMAP data can be requested at <https://www.radc.rush.edu> and downloaded from <https://www.synapse.org> by approved users.

ADGC data is can be requested from NIAGADS at <https://www.niagads.org/resources/related-projects/alzheimers-disease-genetics-consortium-adgc-collection>.

NACC neuropathology data can be requested at <https://nacccdata.org/>.

ACT data can be requested at <https://actagingresearch.org/>.

The results published here are in whole or in part based on data obtained from the AD Knowledge Portal.

GTEx QTL data used is publicly available at <https://www.gtexportal.org/home/datasets>.

ROSMAP QTL data used is publicly available for download at <http://mostafavilab.stat.ubc.ca/xqtl>.

1000 Genomes Phase 3 data is available at <https://www.internationalgenome.org/home>.

Raw long-read RNAseq data generated and utilized in this manuscript are publicly available in both Synapse (<https://www.synapse.org/#!Synapse:syn52047893>) and NIH SRA (accession number: SRP456327; <https://trace.ncbi.nlm.nih.gov/Traces/?view=study&acc=SRP456327>). Processed long-read RNAseq data can be easily downloaded or viewed at https://ebbertlab.com/brain_rna_isoform_seq.html.

Research involving human participants, their data, or biological material

Policy information about studies with [human participants or human data](#). See also policy information about [sex, gender \(identity/presentation\), and sexual orientation](#) and [race, ethnicity and racism](#).

Reporting on sex and gender

Biological sex was used as a covariate in all analyses.

Reporting on race, ethnicity, or other socially relevant groupings

Due to limited sample sizes of participants with substantial non-European descent, we excluded these participants from our study. This was done by merging each of our data sources individually with 1000 Genomes Phase 3 data, performing principal component (PC) analysis, and excluding participants whose positions on a plot of PC1 and PC2 were beyond a distance, determined via visual inspection, from the 1000 Genomes EUR superpopulation centroid.

Population characteristics

We used multiple independent data sets of participants in this study. We adjusted each genetic association analysis for principal components, data source/study, genotyping cohort, sex, and age at death. Demographic details of participants can be found in Table 1. In summary, 53% of participants were female, the mean age of death was 83 years with a SD of 10 years, 48% of participants had at least one APOE e4 allele.

Recruitment

Participants in NACC were recruited at individual Alzheimer's Disease Research Centers, each with its own recruitment criteria. Across different data sources used in this study, participants were recruited from clinics, religious organizations, communities, and hospitals. Participants in NACC have higher prevalence of dementia and APOE e4 than the population at large. ROS recruited priests, brothers, and sisters in the Catholic church who have higher average educational attainment than the general population aged 80 years or older. MAP recruits from community members in the greater Chicago area. ACT recruited residents in the greater Seattle area aged 65 years and older without dementia at time of enrollment.

Ethics oversight

Each study was approved by the respective institutional review boards as appropriate. The IRB of the lead authors on this study deemed that this study did not include human subjects because all research participants were deceased.

Note that full information on the approval of the study protocol must also be provided in the manuscript.

Field-specific reporting

Please select the one below that is the best fit for your research. If you are not sure, read the appropriate sections before making your selection.

Life sciences Behavioural & social sciences Ecological, evolutionary & environmental sciences

For a reference copy of the document with all sections, see nature.com/documents/nr-reporting-summary-flat.pdf

Life sciences study design

All studies must disclose on these points even when the disclosure is negative.

Sample size	Raw data used in this study were collected by the individual studies: neuropathological data: NACC, ACT, ROSMAP; genotype data: ADGC, ROSMAP; RNA-Seq data: ROSMAP; DNA methylation data: ROSMAP. Sample sizes were not pre-determined; all available samples with relevant data that passed quality control and inclusion criteria (see Methods) were included in analyses. The total sample size available for GWAS after QC measures was N=7,463, though sample sizes in individual analyses were smaller based on available phenotype data.
Data exclusions	We excluded samples and variants based on standard quality control procedures for GWAS (Samples: heterozygosity, missingness, and population outliers. Variants: minor allele frequency, missingness, Hardy-Weinberg equilibrium, duplicated variants.) We also excluded participants with rare neuropathological phenotypes (e.g. brain malignancy and traumatic brain injury) that may affect interpretation of neuropathological outcomes used. For RNA-Seq and DNA methylation analyses, we used pre-QCed data from which samples with low RNA integrity scores or bisulfate conversion efficiency had been removed. Complete details of our quality control procedures are available in the Methods and Supplementary Note sections of the manuscript.
Replication	Cerebral amyloid angiopathy (CAA) had previously been studied using an independent cohort from the Mayo Clinical Brain Bank cohort with phenotype, covariate, and genotype data made available on synapse.org. We used 815 available participants to successfully replicate the association between rs7247551 and CAA while adjusting for APOE epsilon diplotypes. We were unable to find suitable replication data sets for other associations because either phenotypes had not been previously studied with GWAS (LATE-NC) or had been studied using a subset of the participants in our study.
Randomization	Each study had different procedures for choosing participants for genotyping, which may have been based on relevant clinical diagnoses if not neuropathological endophenotypes. We adjusted for study and genotyping cohort in all relevant analyses.
Blinding	Genotyping was performed without knowing the neuropathological status of individuals. The analyses were not blinded to the status of individuals because harmonization and quality control procedures required knowing neuropathological status.

Reporting for specific materials, systems and methods

We require information from authors about some types of materials, experimental systems and methods used in many studies. Here, indicate whether each material, system or method listed is relevant to your study. If you are not sure if a list item applies to your research, read the appropriate section before selecting a response.

Materials & experimental systems

n/a	Involved in the study
<input checked="" type="checkbox"/>	<input type="checkbox"/> Antibodies
<input checked="" type="checkbox"/>	<input type="checkbox"/> Eukaryotic cell lines
<input checked="" type="checkbox"/>	<input type="checkbox"/> Palaeontology and archaeology
<input checked="" type="checkbox"/>	<input type="checkbox"/> Animals and other organisms
<input checked="" type="checkbox"/>	<input type="checkbox"/> Clinical data
<input checked="" type="checkbox"/>	<input type="checkbox"/> Dual use research of concern
<input checked="" type="checkbox"/>	<input type="checkbox"/> Plants

Methods

n/a	Involved in the study
<input checked="" type="checkbox"/>	<input type="checkbox"/> ChIP-seq
<input checked="" type="checkbox"/>	<input type="checkbox"/> Flow cytometry
<input checked="" type="checkbox"/>	<input type="checkbox"/> MRI-based neuroimaging